PLOS GENETICS

RESEARCH ARTICLE

# LF4/MOK and a CDK-related kinase regulate the number and length of cilia in *Tetrahymena*

**Yu-Yang Jiang[1], Wolfgang Maier[2], Ralf Baumeister[2], Gregory Minevich[3], Ewa Joachimiak[4], Dorota Wloga[4], Zheng Ruan[5], Natarajan Kannan[5,6], Stephen Bocarro[1], Anoosh Bahraini[1], Krishna Kumar Vasudevan[1], Karl Lechtreck[1], Eduardo Orias[7], Jacek Gaertig[1]***

**1** Department of Cellular Biology, University of Georgia, Athens, Georgia, United States of America, **2** Bio 3/ Bioinformatics and Molecular Genetics, Faculty of Biology and ZBMZ, Faculty of Medicine, Albert-Ludwigs-University of Freiburg, Freiburg, Germany, **3** Department of Biochemistry and Molecular Biophysics, Columbia University Medical Center, New York, New York, United States of America, **4** Laboratory of Cytoskeleton and Cilia Biology, Nencki Institute of Experimental Biology of Polish Academy of Sciences, Warsaw, Poland, **5** Institute of Bioinformatics, University of Georgia, Athens, Georgia, United States of America, **6** Department of Biochemistry and Molecular Biology, University of Georgia, Athens, Georgia, United States of America, **7** Department of Molecular, Cellular and Developmental Biology, University of California Santa Barbara, Santa Barbara, California, United States of America

* jgaertig@uga.edu





**Citation:** Jiang Y-Y, Maier W, Baumeister R, Minevich G, Joachimiak E, Wloga D, et al. (2019) LF4/MOK and a CDK-related kinase regulate the number and length of cilia in *Tetrahymena*. PLoS Genet 15(7): e1008099. https://doi.org/10.1371/journal.pgen.1008099

**Editor:** Susan K. Dutcher, Washington University School of Medicine, UNITED STATES

**Received:** March 15, 2019

**Accepted:** June 13, 2019

**Published:** July 24, 2019



**Data Availability Statement:** All relevant data are within the manuscript and its Supporting Information files

**Funding:** This work was supported by the NIH National Institute of Child Health and Human Development R21HD092809 (to JG) and NIH National Institute of General Medical Sciences 5RO1GM114409 (to NK), a bridge funding from the Office of the Vice-President for Research and the Department of Cellular Biology at the University of Georgia (to JG), the National Science Foundation

## Abstract

The length of cilia is controlled by a poorly understood mechanism that involves members of the conserved RCK kinase group, and among them, the LF4/MOK kinases. The multiciliated protist model, *Tetrahymena*, carries two types of cilia (oral and locomotory) and the length of the locomotory cilia is dependent on their position with the cell. In *Tetrahymena*, loss of an LF4/MOK ortholog, LF4A, lengthened the locomotory cilia, but also reduced their number. Without LF4A, cilia assembled faster and showed signs of increased intraflagellar transport (IFT). Consistently, overproduced LF4A shortened cilia and downregulated IFT. GFP-tagged LF4A, expressed in the native locus and imaged by total internal reflection microscopy, was enriched at the basal bodies and distributed along the shafts of cilia. Within cilia, most LF4A-GFP particles were immobile and a few either diffused or moved by IFT. We suggest that the distribution of LF4/MOK along the cilium delivers a uniform dose of inhibition to IFT trains that travel from the base to the tip. In a longer cilium, the IFT machinery may experience a higher cumulative dose of inhibition by LF4/MOK. Thus, LF4/MOK activity could be a readout of cilium length that helps to balance the rate of IFT-driven assembly with the rate of disassembly at steady state. We used a forward genetic screen to identify a CDK-related kinase, CDKR1, whose loss-of-function suppressed the shortening of cilia caused by overexpression of LF4A, by reducing its kinase activity. Loss of CDKR1 alone lengthened both the locomotory and oral cilia. CDKR1 resembles other known ciliary CDK-related kinases: LF2 of *Chlamydomonas*, mammalian CCRK and DYF-18 of *C. elegans*, in lacking the cyclin-binding motif and acting upstream of RCKs. The new genetic tools we developed here for *Tetrahymena* have potential for further dissection of the principles of cilia length regulation in multiciliated cells.

grant MCB-1149106 (to NK), grants from Deutsche Forschungsgemeinschaft BIOSS CRC746 and CRC850 (to RB), and grants from the National Science Centre, Poland: OPUS13 2017/25/B/NZ3/01609 (to DW) and OPUS15 2018/29/B/NZ3/02443 (to EJ). GM was supported by a pre-doctoral fellowship from the NIH National Institute of Neurological Disorders and Stroke (1F31NS074841-01). The funders had no role in study design, data collection and analysis, decision to publish, or preparation of the manuscript

**Competing interests:** The authors have declared no competing interests exist.

## Author summary

Cilia are conserved organelles that generate motility and mediate vital sensory functions, including olfaction and vision. Cilia that are either too short or too long fail to generate proper forces or responses to extracellular signals. Several cilia-based diseases (ciliopathies) are associated with defects in cilia length. We used the multiciliated model protist *Tetrahymena*, to study a conserved protein kinase whose activity shortens cilia, LF4/MOK. We find that cells lacking a LF4/MOK kinase of *Tetrahymena*, LF4A, have excessively long, but also fewer cilia. We show that LF4A decreases intraflagellar transport, a mechanism that shuttles ciliary precursors from the cilium base to the tip. Live imaging revealed that LF4A is distributed along the entire length of the cilium and remains mostly immobile, likely due to its anchoring to ciliary microtubules. We speculate that in longer cilia, the intraflagellar transport machinery is exposed to a higher dose of inhibition by LF4A, which could decrease the rate of cilium assembly, to balance the rate of cilium disassembly in mature cilia that maintain stable length. We use a genetic screen to identify another kinase, CDKR1, as an activator of LF4A. The new tools described here should be useful in further dissection of the principles of cilia length regulation in multiciliated cells.

## Introduction

The classical "long-zero" experiment in the green flagellate *Chlamydomonas reinhardtii* revealed that the length of cilia is sensed and actively maintained [1]. When one of the two cilia of *Chlamydomonas* was removed, the intact cilium immediately started to shorten, while the amputated cilium started to regrow. When both cilia reached about the same intermediate length, they continued to elongate at the same rate, to achieve an equal steady-state length [1]. A number of ciliopathies including Joubert syndrome [2], Meckel syndrome [3, 4], endocrine-cerebro-osteodysplasia syndrome [5, 6], short rib polydactyly syndrome [7, 8], retinitis pigmentosa [9, 10], non-syndromic recessive deafness [11], polycystic kidney disease [12, 13] and juvenile epilepsy [14] are caused by mutations in proteins that affect cilium length.

The assembly of most cilia involves delivery of precursors from the cell body to the ciliary base, followed by their distribution along the length of the cilium by the intraflagellar transport (IFT) pathway [15]. During IFT, motor proteins move large protein complexes, IFT trains, that in turn ferry precursors of cilia, including tubulin, along axonemal microtubules [16–18]. Kinesin-2 is the IFT motor that operates in the anterograde direction, from the cilium base to the distal tip, where most of the precursors are incorporated into the axoneme [19, 20]. IFT dynein (dynein-2) returns IFT trains and components that turn-over back to the ciliary base [21–23]. The cilium disassembly pathway involves kinesin-related microtubule end destabilizers [24–28], and protein modifications including glutamylation [29], ubiquitination [30, 31] and phosphorylation (reviewed in [32]). In a mature cilium, its steady-state length results from a balance between the rates of assembly (mediated by IFT) and disassembly [33]. Importantly, IFT changes as a function of cilium assembly status. In *Chlamydomonas*, the IFT train size [34, 35] and cargo load [16, 17, 36] are higher in assembling cilia as compared to steady-state or disassembling cilia. On the other hand, also in *Chlamydomonas*, the disassembly rate increases in cilia that are abnormally long [37]. These observations suggest that there are mechanisms that sense and adjust cilium length by controlling the rates of cilia assembly (IFT) and disassembly.

Several conserved kinases negatively regulate cilium length (their loss makes cilia longer) including: two subgroups of the ROS cross-hybridizing kinases (RCKs): LF4/MOK [37–40]

and DYF-5/ICK/MAK [38, 41–46], CDK-related kinases: LF2/CCRK and DYF-18 [43, 46–48], NRK/NEK [37, 49–52] and LF5/CDKL5 [53]. Consistently, inhibition of protein phosphatases (PP1 and PP2A) shortens cilia [54–57]. On the other hand, CDK5 in mammals [58, 59] and a calcium-dependent kinase CDPK1 in *Chlamydomonas* [60], promote cilia assembly as their losses make cilia shorter. CDPK1 promotes cilia assembly by increasing the turnaround of IFT trains at the ciliary tip [60]. However, CDPK1 also decreases the assembly rate by reducing the entry of IFT trains into the cilium [60].

Recent reports have linked some cilium length-regulating kinases to the anterograde IFT motor, kinesin-2. In *Chlamydomonas*, CDPK1 phosphorylates the tail domain of the motor subunit of kinesin-2 (FLA8) and a non-phosphorylatable substitution at this phosphorylation site (S663A) inhibits association of kinesin-2 with IFT complexes and reduces their entry into cilia [60]. In *C. elegans*, loss-of-function mutations in an RCK DYF-5, and a CDK-related DYF-18, rescue defective ciliogenesis caused by an autoinhibitory mutation in the kinesin-2 motor OSM-3, suggesting that DYF-5 and DYF-18 inhibit kinesin-2 [46].

It remains unclear how cilium length is sensed and translated into proper modulations of the rates of cilium assembly and disassembly. The majority of published studies on the control of cilia length have been done in *Chlamydomonas reinhardtii* that carries two cilia, and in animal cells with single primary cilia (reviewed in [61–63]) and less is known about how cilium length is regulated in multiciliated cells, such as the ciliate *Tetrahymena thermophila* used here.

In *Chlamydomonas*, loss of LF4 (long flagella protein 4, an ortholog of the mammalian MOK) makes cilia twice as long as in the wild type [39, 64], increases the amount of IFT proteins entering the cilium [35] and increases the rates of both cilium assembly and disassembly [37]. Here we investigate the significance of LF4/MOK in the multiciliated *Tetrahymena*. A single *Tetrahymena* cell carries between 500–1000 cilia, including oral cilia that support phagocytosis, and locomotory cilia that are arranged in ~20 longitudinal rows (reviewed in [65]). Importantly, in *Tetrahymena*, both the time of assembly and length are dependent on cilium type (oral versus locomotory) and position on the anteroposterior cell axis [50, 66, 67]. We find here that *Tetrahymena* has a single cilia-associated LF4/MOK kinase, LF4A, which negatively regulates the length, and positively regulates the number of locomotory cilia. We use a forward genetic screen to identify a CDK-type kinase, CDKR1, as an activator of LF4/MOK, which regulates the length of both locomotory and oral cilia. Our data suggest that specific cilium length-regulating kinases regulate subsets of cilia in the same multiciliated cell.

## Results

### LF4A both shortens cilia and promotes ciliogenesis in *Tetrahymena*

The CMGC (CDK, MAP, GSK, CDK-like [68]) kinase family contains several conserved subfamilies whose members affect cilium length including: RCKs (subdivided into LF4/MOK and DYF-5/MAK/ICK groups), CDK-related kinases (LF2/CCRK and DYF-18) and LF5/CDKL5 kinases. We performed a phylogenetic analysis of the cilia-associated CMGC kinases of *Tetrahymena thermophila* and several other ciliated and nonciliated species. The genome of *Tetrahymena* encodes members of each of the cilia-associated CMGC subfamily except for LF2/CCRK (Fig 1A). However, among the CDK-related kinases, TTHERM_01080590 protein (that we will later rename CDKR1, see below) groups with DYF-18 of *C. elegans* that was suggested to be a homolog of LF2/CCRKs [46, 48]. Among the RCKs, *Tetrahymena* has seven DYF-5/MAK/ICK type kinases and two LF4/MOK kinases: LF4A (TTHERM_00058800) and LF4B (TTHERM_00822360). While LF4A acts in cilia, surprisingly, LF4B appears to be expressed only during the sexual process of conjugation, where it likely plays a non-ciliary role (see below and S1 Fig).

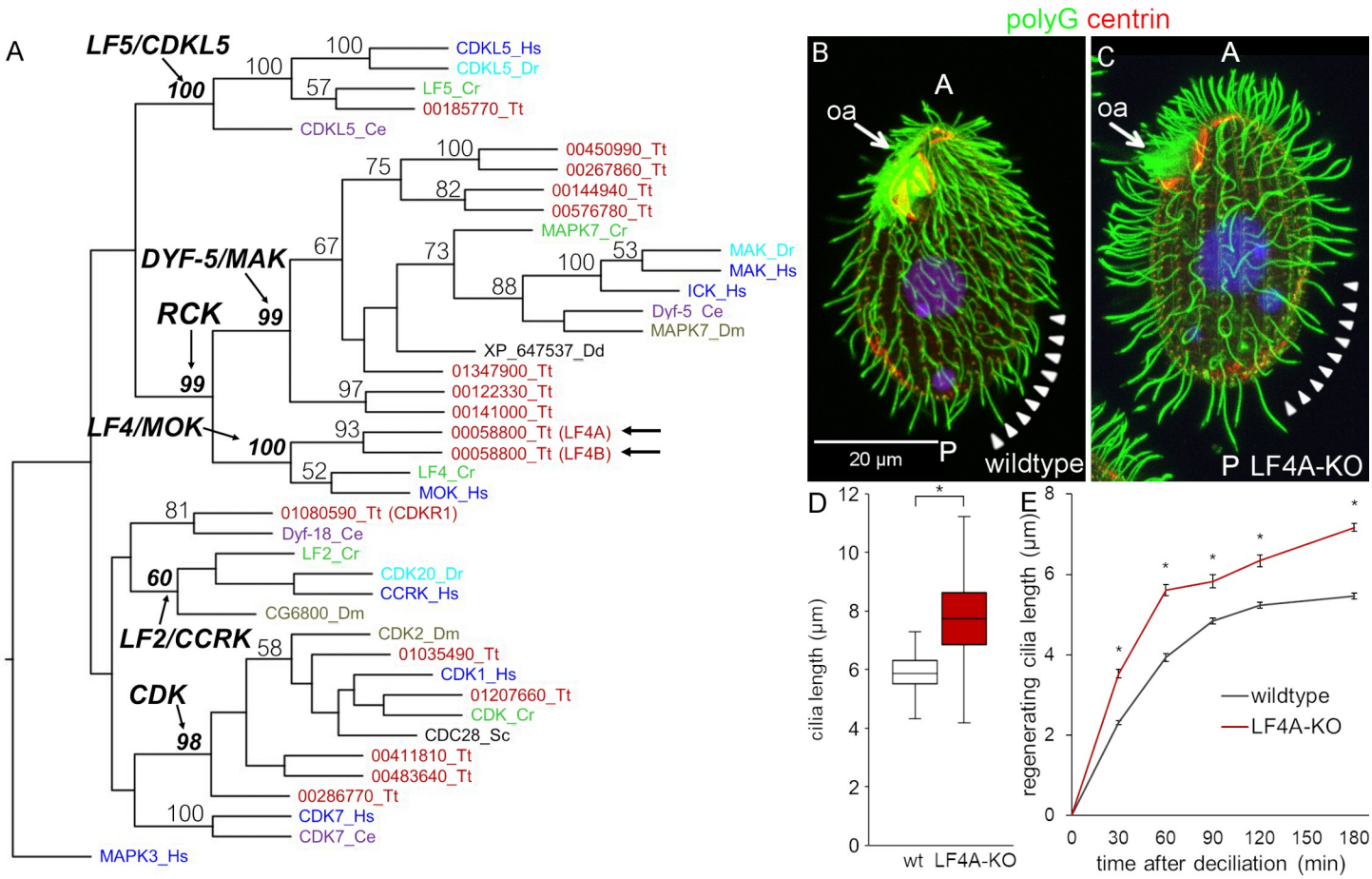


**Fig 1. *LF4A* regulates cilia length and number in *Tetrahymena*.** (A) A neighbor joining phylogenetic tree of a subset of CMGC kinases. The human MAPK3 was used as an outgroup. The numbers on the branches represent bootstrap support values above 50%. Arrows mark the two LF4/MOK homologs of *Tetrahymena*. (B and C) A wild-type (B) and an LF4A-KO cell (C) stained with the anti-polyG tubulin antibodies to visualize cilia (green), anti-centrin antibody 20H5 to mark the basal bodies (red) and DAPI (blue). Arrowheads indicate the posterior-dorsal region that is less densely ciliated in LF4A-KO. Abbreviations: oa, oral apparatus; A, anterior cell end; P, posterior cell end. (D) A box and whisker plot of locomotory cilia length. Cilia from ten wildtype and ten LF4A-KO cells were measured. The average cilium length for the wild type (n = 216) is 5.88 μm, SD (standard deviation): 0.38 μm; LF4A-KO (n = 367) 7.74 μm, SD: 1.82 μm. $p < 0.01$. (E) The length of cilia during regeneration after deciliation by pH shock. Four to 6 cells, 50–150 cilia were measured at each time point. Asterisks (*) indicate significant differences ($p < 0.01$ at each indicated time point).

https://doi.org/10.1371/journal.pgen.1008099.g001

We constructed *Tetrahymena* cells homozygous for a disruption of the *LF4A* gene (LF4A-KO strain). The LF4A-KO cells assembled fewer locomotory cilia (especially in the posterior/dorsal region) that were 32% longer, compared to the wild type (Fig 1B–1D). In the wild type, cilium length gradually increases from the anterior to the posterior cell end ([50] and Fig 1B). Such a length gradient was also apparent in the LF4A-KO cells despite the overall lengthening of cilia (Fig 1C). The length of oral cilia appeared unaffected (Fig 1B and 1C, arrows). In *Chlamydomonas*, LF4 decreases the rate of cilia assembly [35, 37]. In agreement, following deciliation of *Tetrahymena* by a pH shock, the locomotory cilia grew faster in LF4A-KO than in the wild type (Fig 1E).

## Inside cilia, LF4A-GFP is mostly stationary and rarely diffuses or moves as IFT cargo

We added GFP to the C-terminus of LF4A, by engineering its gene (to preserve expression under the native promoter). Based on immunofluorescence, LF4A-GFP was strongly present

at the ciliary bases (both oral and locomotory) and scattered along the shafts of locomotory cilia (Fig 2B compare to Fig 2A). Total internal reflection fluorescence microscopy (TIRFM) confirmed the presence of LF4A-GFP at the ciliary bases and along the shafts of locomotory cilia (Fig 2D). In live cells imaged by TIRFM, most of LF4A-GFP particles were immobile and a few either diffused or moved along linear tracks with IFT velocities (in either anterograde or retrograde direction (Fig 2E, arrows). The mobile LF4A-GFP particles were rare: not more than a few percent of cilia per cell had convincingly mobile LF4A-GFP and even inside these

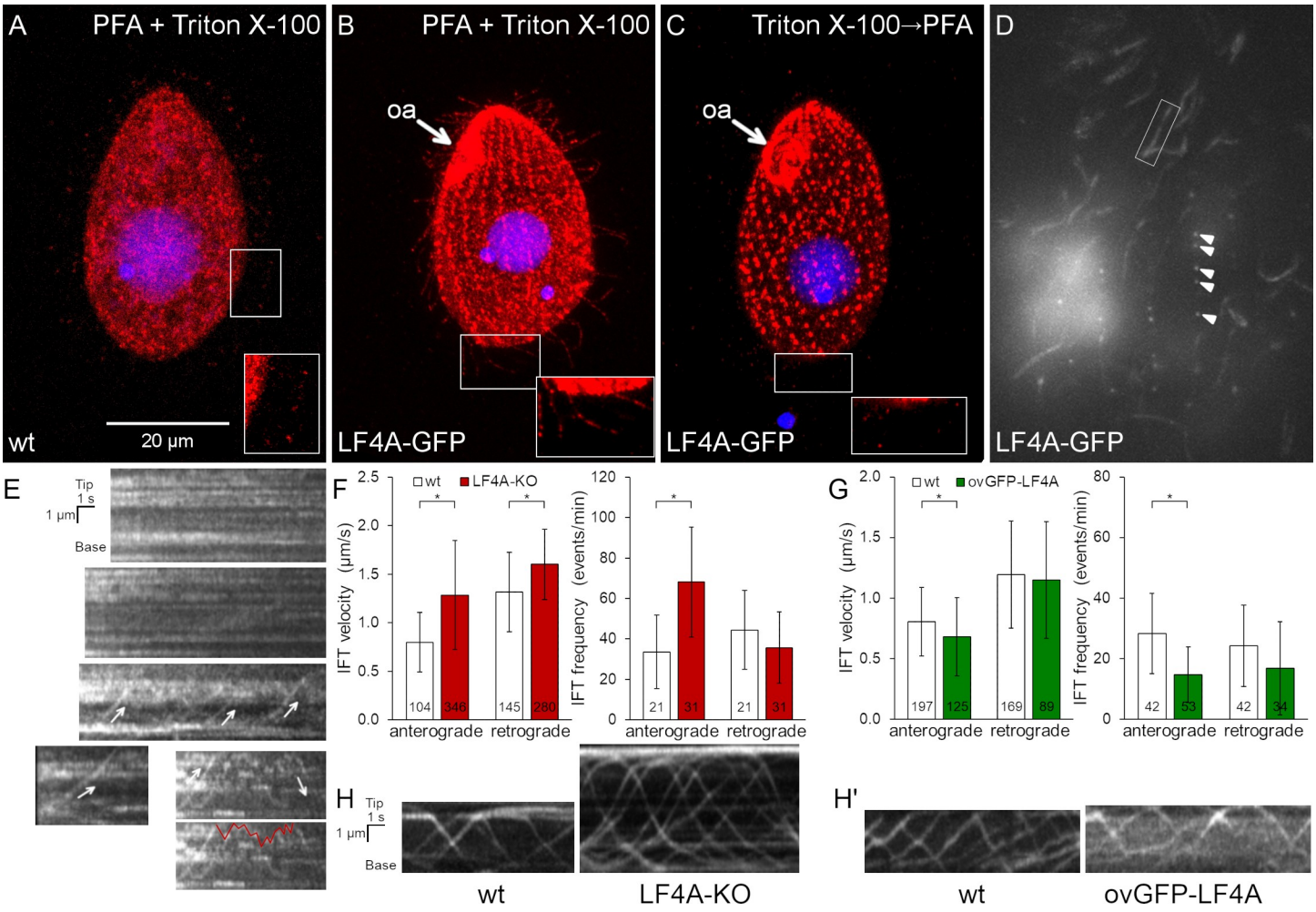


**Fig 2. LF4A-GFP localizes to the basal bodies and along cilia, is transported by IFT and affects IFT.** (A-B) A wild-type (negative control non-GFP expressing) cell (A) and a cell expressing LF4A-GFP under the native promoter (B) were subjected to simultaneous fixation/permeabilization (using a mixture of paraformaldehyde and Triton X-100) and stained with the anti-GFP antibodies (red) and DAPI (blue). In the negative control, the red background (anti-GFP) signal is in the cell body and occasionally at the tips of cilia (A inset). Specific LF4A-GFP signal is present near the basal bodies and along the shafts of locomotory cilia (B inset compare to A inset). (C) An LF4A-GFP expressing cell that was first permeabilized (with Triton X-100) and then fixed (with paraformaldehyde) prior to immunofluorescence. Compared to (B), the LF4A-GFP signal remained strong near the basal bodies but is decreased in cilia. (D) A TIRFM image of a live LF4A-GFP-expressing cell. Arrowheads indicate several basal bodies within a locomotory row, the box highlights an example of a ciliary shaft. (E) Five representative examples of kymographs obtained from the TIRFM videos of LF4A-GFP cells. In most cilia, LF4A-GFP particles are stationary and some move with velocities similar to IFT velocities (arrows) or diffuse (an example of a diffusion event is marked with a red line on the duplicate of the bottom right kymograph). (F) The IFT velocities (left) and IFT event frequencies (right) in cilia of either wild-type or LF4A-KO cells that express DYF1-GFP, an IFT reporter. (G) The IFT velocities (left) and event frequencies (right) in cilia of either wild-type or GFP-LF4A-overexpressing cells. Both strains were exposed to $Cd^{2+}$ for 3 hours. In (F) and (G), the sample sizes are indicated, asterisks mark significant differences (one way Anova $p<0.01$), error bars represent SDs. (H) Examples of kymographs of GFP-DYF1 in cilia of either wild-type or LF4A-KO cells corresponding to the data shown in panel F. (H') Examples of kymographs of GFP-DYF1 in either wild-type or GFP-LF4A overproducing cells corresponding to the data shown in panel G. Abbreviations: oa, oral apparatus; PFA, paraformaldehyde.

https://doi.org/10.1371/journal.pgen.1008099.g002

cilia most of LF4A-GFP particles remained immobile (S1 Video). This contrasts with the behavior of fluorescently tagged IFT proteins, most of which were mobile under the same imaging conditions (Figs 2H, 2H' and 3H). Thus, most of LF4A may be anchored in the cilium. Based on immunofluorescence, the signal of LF4A-GFP in the ciliary shafts (but not at the basal bodies) greatly decreased after extraction with Triton X-100 (Fig 2C compare to Fig 2B), indicating that the suggested anchorage of LF4A is relatively weak.

The apparent paralog of LF4A, LF4B (Fig 1A) does not appear to be associated with cilia. LF4B-GFP was not detectable in the vegetatively-growing cells (S1A Fig). In the early phase of conjugation, LF4B-GFP localized to the junction between the two mating cells (S1B and S1C Fig), in a pattern that did not correspond to the positions of cilia near the conjugal junction [69–71]. Consistently, while the mRNA of *LF4A* is abundant in the vegetatively-growing cells, the mRNA of *LF4B* is present above the background only during the early stage of conjugation (S1D Fig, data from [72]). Likely, *Tetrahymena* has only a single cilia-associated LF4/MOK, LF4A.

## LF4A kinase activity shortens cilia and downregulates IFT

We overproduced GFP-LF4A, using the $Cd^{2+}$-inducible MTT1 promoter [73]. After 6 or more hours of exposure to added $Cd^{2+}$, GFP-LF4A strongly accumulated at the bases of both oral and locomotory cilia, and all cilia shortened to become stumps (Fig 3B compare to the GFP negative control in Fig 3A and 3F), and the GFP-LF4A-overproducing cells became paralyzed. In addition, based on TIRFM, overproduced GFP-LF4A decorated two non-ciliary microtubule-based structures: longitudinal microtubule bundles and contractile vacuole pores (S2A Fig, left panel), which suggests that LF4A has a microtubule-binding affinity. With time, the GFP-LF4A-overproducing cells became excessively large and misshaped (Fig 3D), indicating defects in cytokinesis. This is not surprising because in *Tetrahymena* locomotory cilia are required for the scission of daughter cells at the end of cytokinesis [74].

*In vitro*, LF4 of *Chlamydomonas* phosphorylates a generic substrate of serine/threonine kinases, myelin basic protein (MBP) and autophosphorylates [39]. Likewise, GFP-LF4A pulled down from overproducing *Tetrahymena*, phosphorylated MBP and itself *in vitro* (Fig 3E). An overproduced GFP-LF4A with a substitution of the conserved F82 (gatekeeper residue), GFP-LF4A$^{F82A}$, had greatly reduced kinase activity *in vitro* (Fig 3E) and did not shorten cilia *in vivo* (Fig 3C and 3F). While the overproduced GFP-LF4A accumulated at the ciliary bases (Figs 3B and S2A left panel), the kinase-weak GFP-LF4A$^{F82A}$ accumulated at the tips of cilia (Figs 3C and S2A middle panel). Overproduced mCherry-LF4A$^{F82A}$ accumulated in cilia, but unlike GFP-LF4A$^{F82A}$ was not enriched at the ciliary tips (S2A Fig right panel, S2C Fig middle and right panel). Thus, the tip enrichment of GFP-LF4A$^{F82A}$ is likely an artifact of the GFP tag, possibly caused by oligomerization of GFP [75]. Inside cilia, the particles of overproduced mCherry-LF4A and mCherry-LF4A$^{F82A}$ were either immobile or moved with the IFT trains (S2B Fig). Thus, the kinase activity of LF4A is required for its cilia-shortening activity but is not required for its entry into cilia, anchorage or transport by IFT.

It is intriguing that only the kinase weak and not the active version of GFP-LF4A accumulated at the ciliary tips (Figs 3B, 3C and S2A). The overproduced GFP-LF4A may fail to build up at the ciliary tips, if its kinase activity blocks the anterograde IFT of cargoes, including GFP-LF4A itself. Thus, we examined how the levels of LF4A affect IFT. In cells expressing a tagged IFT subcomplex B protein, GFP-DYF1/IFT70 [76, 77], the loss of LF4A significantly increased the velocities of both the anterograde and retrograde IFT (Fig 2F and 2H). Overexpression of GFP-LF4A mildly decelerated the anterograde but not retrograde IFT (Fig 2G and 2H'). Overproduced mCherry-LF4A (but not mCherry-LF4A$^{F82A}$) decreased the velocities of both the anterograde and retrograde IFT based on imaging of a tagged IFT subcomplex A

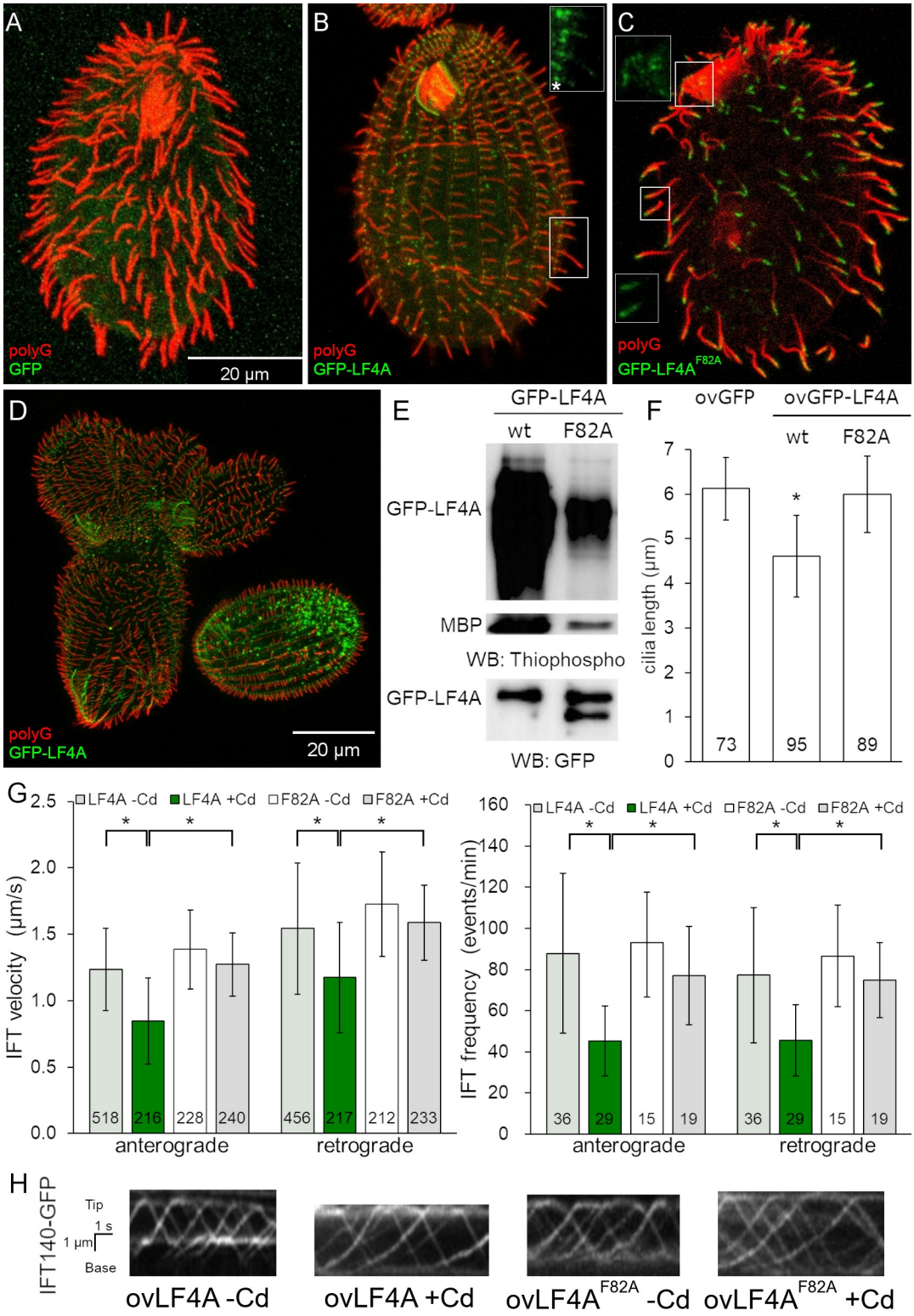


**Fig 3. Excessive LF4A kinase activity shortens cilia and decreases IFT.** (A-C) Cells (treated with 2.5 μg/ml $CdCl_2$ for 6 hours) overexpressing either GFP (A), GFP-LF4A (B) or GFP-LF4A$^{F82A}$ (C) showing GFP fluorescence (green) and labeled by the anti-polyG tubulin antibodies to visualize cilia (red). The shortening of cilia is evident only in the cell expressing GFP-LF4A (B) where it is enriched at the basal bodies (asterisk). GFP-LF4A$^{F82A}$ accumulates at the tips of cilia (C). The insets in B-C show the green signal of GFP-LF4A alone at higher magnification. (D) GFP-LF4A-overexpressing cells after overnight

induction with $Cd^{2+}$, have short cilia, are large and irregular in shape, consistent with cytokinesis defects. (E) The results of an *in vitro* kinase assay with either GFP-LF4A or GFP-$LF4^{F82A}$. Each protein was overexpressed in *Tetrahymena* and purified on anti-GFP-beads. The beads were incubated with the recombinant myelin basic protein (MBP) and ATP-γ-S. The phosphorylated products were detected on a western blot probed with the anti-thiophosphorylation antibody 51–8; the upper and middle panels show sections of the same blot containing autophosphorylated GFP-LF4A and MBP, respectively. The same amounts of IP inputs were analyzed on a separate western blot probed the anti-GFP antibodies and shown in the bottom panel (WB: GFP); the lower band in the right lane likely is a proteolytic degradation product of GFP-LF4A. (F) The lengths of locomotory cilia of cells that overproduce (for 3 hours) either GFP, GFP-LF4A or the kinase-weak GFP-$LF4A^{F82A}$. The cilia lengths in the GFP and GFP-$LF4A^{F82A}$ cells were not significantly different ($p > 0.01$), while the GFP-LF4A cilia were significantly reduced (~75% of the length of GFP controls, one way Anova test, $p < 0.01$). Sample sizes are indicated, error bars represent SDs. (G) The anterograde and retrograde IFT velocities and frequencies in cilia of cells that express IFT140-GFP and overexpress either mCherry-LF4A or mCherry-$LF4A^{F82A}$. The IFT speeds are significantly reduced in mCherry-LF4A as compared to mCherry-$LF4A^{F82A}$ overexpressing cells (exposed to added $Cd^{2+}$ for 3 hours). The sample sizes (numbers of tracks measured) are indicated, asterisks indicate statistically significant differences (one way Anova, $p<0.01$), error bars represent SDs. (H) Examples of kymographs of cilia in cells expressing IFT140-GFP in different genetic backgrounds and conditions corresponding to the data shown in panel G. Scale bar: 1 μm x 1 s.

https://doi.org/10.1371/journal.pgen.1008099.g003

subunit IFT140 [19, 78], IFT140-GFP (Fig 3G left panel, Fig 3H). In addition, the loss of LF4A significantly increased the frequency of the anterograde (but not the retrograde) IFT events (Fig 2F right panel). Overexpression of GFP-LF4A strongly reduced the IFT event frequencies in the anterograde direction in cells with GFP-DYF1 reporter (Fig 2G right panel, Fig 2H', S2 and S3 Videos) while overexpression of mCherry-LF4A (but not mCherry-$LF4A^{F82A}$) decreased IFT frequency in both directions in cells expressing IFT140-GFP (Fig 3G right panel, Fig 3H). Overall these observations indicate that LF4A decreases IFT by reducing both the frequency and velocity of IFT trains.

## Identification of an *LF4A* interactor, CDKR1

To find potential interactors of LF4/MOK, we performed a genetic screen for suppressors of GFP-LF4A overexpression, taking advantage of the resulting cell paralysis. We introduced a GFP-LF4A transgene operating under the MTT1 promoter and linked to the *neo5* marker (ovGFP-lf4a allele) into the (germline) micronucleus, by replacing the native *LF4A* locus (Figs 4A and S3). The transgene-carrying strain was mutagenized with nitrosoguanidine and subjected to self-fertilization by uniparental cytogamy [79]. This procedure generates whole genome homozygotes, each derived from a single, diploidized meiotic product of the parent cell, and thus allows for isolation of recessive and dominant mutations. $Cd^{2+}$ was added to the mutagenized progeny to induce overexpression of GFP-LF4A and to paralyze the non-suppressed progeny. Suppressors were isolated based on their capacity to swim to the top of test tubes (Fig 4B). Five independent suppressor clones (designated as F0 generation clones) were isolated, while none were found among the progeny of a similar number (~$3 \times 10^7$) of non-mutagenized cells. To distinguish between the extragenic and intragenic suppressions, we tested each suppressor phenotype for linkage with the transgene-coupled *neo5* marker that confers resistance to paromomycin. The F0s were crossed to a wild type and the F1 heterozygous progeny were used to generate F2s by self-fertilization. Tight linkage (essentially 0% recombinants) was expected for an intragenic suppressor mutation while a completely unlinked single suppressor mutation would yield a 1:1 ratio of recombinant to parental F2 genotypes (Figs 4C and S3). Four suppressor clones (SUP2,3,4 and 5) were judged to be intragenic, and one suppressor clone (SUP1) was judged to be extragenic, based on the ~1:2 ratio of the parental versus recombinant F2 phenotypes (the excess of recombinants could be spurious, due to unequal growth rates of suppressed and unsuppressed F2 progeny).

When the four intragenic suppressors were exposed to $Cd^{2+}$ to induce overproduction of GFP-LF4A, SUP2 lacked a GFP signal while SUP3, SUP4 and SUP5 had a strong GFP-LF4A

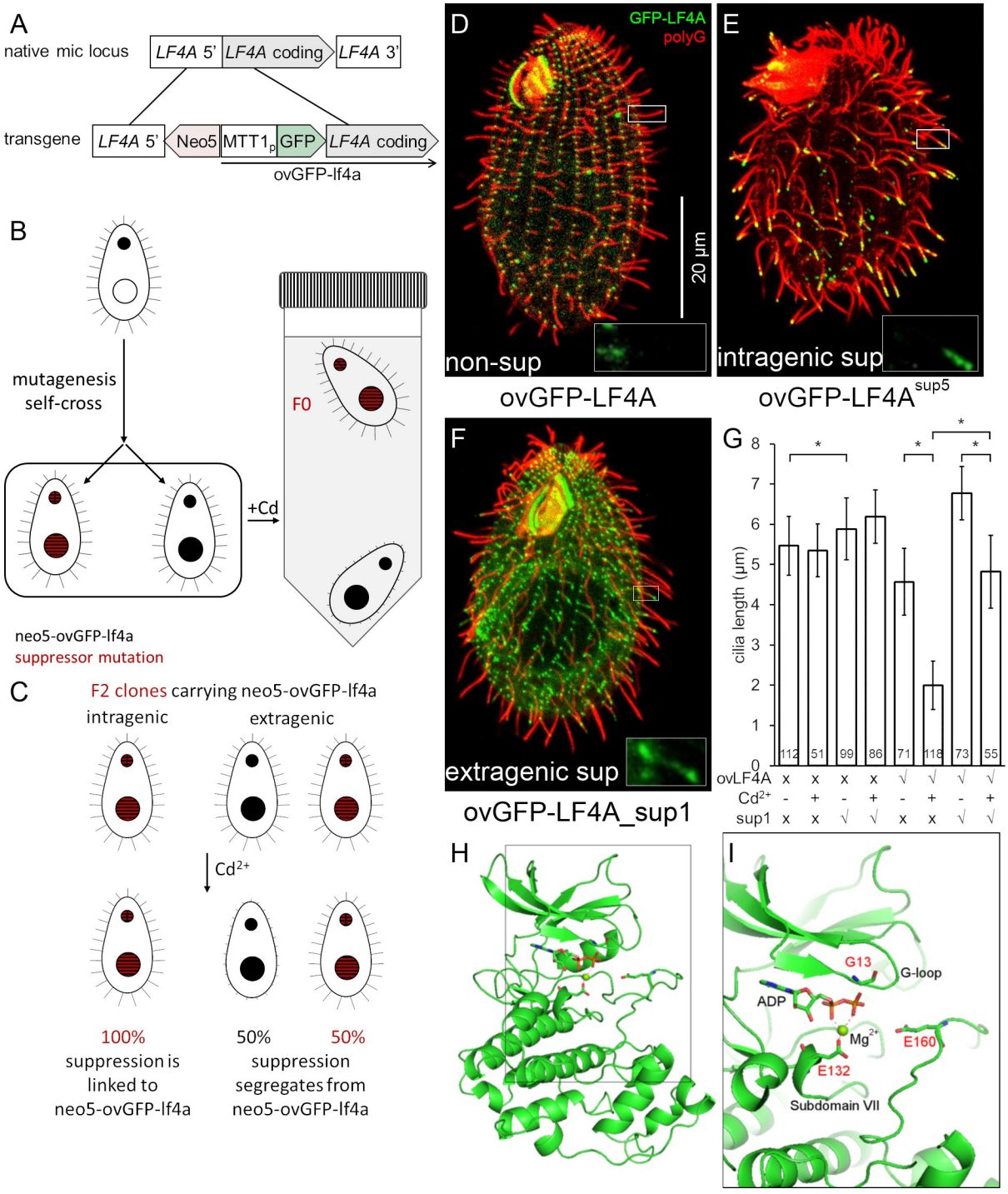


**Fig 4. Isolation of intragenic and extragenic suppressors of GFP-LF4A overexpression.** (A-C) The pipeline used for identification of intragenic and extragenic suppressors of overexpression of GFP-LF4A. (A) The structure of the transgene that was placed in the micronucleus. The transgene uses MTT1 promoter to express GFP-LF4A. A *neo5* cassette is closely linked. The transgene replaces the endogenous *LF4A*. (B) An outline of the procedure for generating suppressors. A heterokaryon with the ovGFP-lf4a transgene in the micronucleus (solid black) was subjected to mutagenesis and a self-fertilizing cross. The homozygous progeny was selected based on paromomycin resistance conferred by *neo5* and some progeny clones may carry a suppressor mutation (red stripes). The progeny cells were treated with $Cd^{2+}$ in tubes kept in vertical position. The progeny clones that lack a suppressor mutation shorten cilia and sink to the tube bottom. The suppressors (F0) remain motile and accumulate near the top of the tube due to negative gravitaxis. (C) The principle of testing whether the suppression is intra- or extragenic (for details see S3 Fig). The F1 clones were subjected to a self-cross and the pm-r F2 progeny clones were isolated. An intragenic suppressor gives pm-r F2 progeny clones that are 100% motile (suppressed), as the suppression is linked to the transgene. An extragenic

suppressor generates F2 pm-r clones that are either suppressed (motile) or not (paralyzed). (D-F) Cells that were exposed for 6 hours to $Cd^{2+}$ to induce GFP-LF4A, subjected to immunofluorescence to reveal GFP (green) and polyG tubulin (red). Insets show the GFP-LF4A signal alone in examples of cilia at a higher magnification. (D) A non-mutagenized non-suppressed cell; GFP-LF4A is enriched at the bases of cilia. (E) An intragenic suppressor cell (SUP5); GFP-LF4A is enriched at the tips of both oral and locomotory cilia. (F) An extragenic suppressor cell (SUP1); GFP-LF4A is prominent at the bases, at the distal ends and along the ciliary shafts in short (presumably assembling) cilia. (G) The locomotory cilia length of F2 clones of four genotypes without and with 6 hours $Cd^{2+}$ treatment. Sample sizes (number of cilia measured) are indicated, asterisks indicate a statistically significant difference (one way Anova $p<0.01$), error bars indicate SDs. (H) A 3D predicted structure of the kinase domain of LF4A based on homology-directed modeling using CDK of *Cryptosporidium* (Chain A of PDB 3NIZ) as template. (I) A zoomed-in view of a region of the structure showing three locations of substitutions (shown as sticks) found in the intragenic suppressors sup3 (E132K), sup4 (G13S) and sup5 (E160K).

https://doi.org/10.1371/journal.pgen.1008099.g004

signal at the tips of cilia (Fig 4E compare to the non-suppressed cell in Figs 4D and S4), as seen earlier for GFP-LF4A$^{F82A}$ (Fig 3C). The extragenic suppressor, SUP1, had GFP-LF4A at the ciliary bases, but also along the length and at the tips of short (presumably assembling) cilia (Fig 4F).

Sanger DNA sequencing of the ovGFP-LF4A transgene in SUP2 revealed multiple mutations in the MTT1 and GFP portions of the transgene, consistent with the lack of GFP fluorescence. SUP3, SUP4 and SUP5 carried single point mutations, predicted to result in E132K, G13S and E160K substitutions, respectively, in the kinase domain of LF4A. A homology-based model of the LF4A kinase domain (using the 3D structure of CDK of *Cryptosporidium* (Chain A of PDB 3NIZ) as a template [80, 81]) revealed that all three affected amino acids are adjacent to the kinase active site (Fig 4H and 4I). While it is not clear how these mutations affect LF4A, in other kinase types substitutions at the positions equivalent to G13 and E132 are associated with diseases [82].

To identify the causal mutation in the single extragenic suppressor SUP1, we used comparative whole-genome sequencing as recently described [83]. A number of independent (meiotic segregant) F2 clones, all derived from a single sup1/SUP1$^{+}$ heterozygote, were combined into a suppressed and a non-suppressed pool (Fig 5A and 5B) and the pooled genomic DNAs were sequenced. The sequence variants found in the suppressed pool were subjected to bioinformatic subtractions (to remove variants also found in the unsuppressed pool and in other unrelated strains) and filtering (for nitrosoguanidine-type mutations [84]) (Fig 5C). These steps yielded three variants, each located on a different micronuclear chromosome (S1 Table). We also used the "allelic composition contrast analysis (ACCA)" to plot the frequency of variant co-segregation with the suppression phenotype along each of the five micronuclear chromosomes [83]. A single peak of linkage was present on the micronuclear chromosome 3 at a bp location between 9 to 10 Mb (Fig 5E), a region that intersected with one of the three variants identified by subtractions and filtration: the T to C mutation on macronuclear scaffold 8254401 at bp location 105680, in the gene *TTHERM_01080590*, which encodes a kinase. The mutation changes the predicted stop into a tryptophan codon and adds a "WIRNLLILNG" sequence to the otherwise normal C-terminus of TTHERM_01080590 protein (Fig 5D). Based on a kinase profiling search [85, 86], TTHERM_01080590 is a CDK-related kinase and therefore we named the *TTHERM_01080590* gene *CDKR1* (cyclin-dependent kinase-related 1). Among several metazoan species analyzed, CDKR1 is most similar to DYF-18 (Fig 1A), a known cilia-associated CDK-related kinase of *C. elegans*, which was proposed to be a homolog of LF2/CCRK CDK kinases [46, 48]. While our phylogenetic analysis does not support either DYF-18 or CDKR1 as orthologs of LF2/CCRK, we note that DYF-18, CDKR1, LF2 and CCRK are all CDK-type kinases that lack the cyclin-binding motif, PSTAIRE, characteristic of the canonical CDKs that regulate the cell cycle (S5C Fig), and are all associated with cilia where they act upstream of RCKs (see below and [40, 43, 47, 48, 64]).

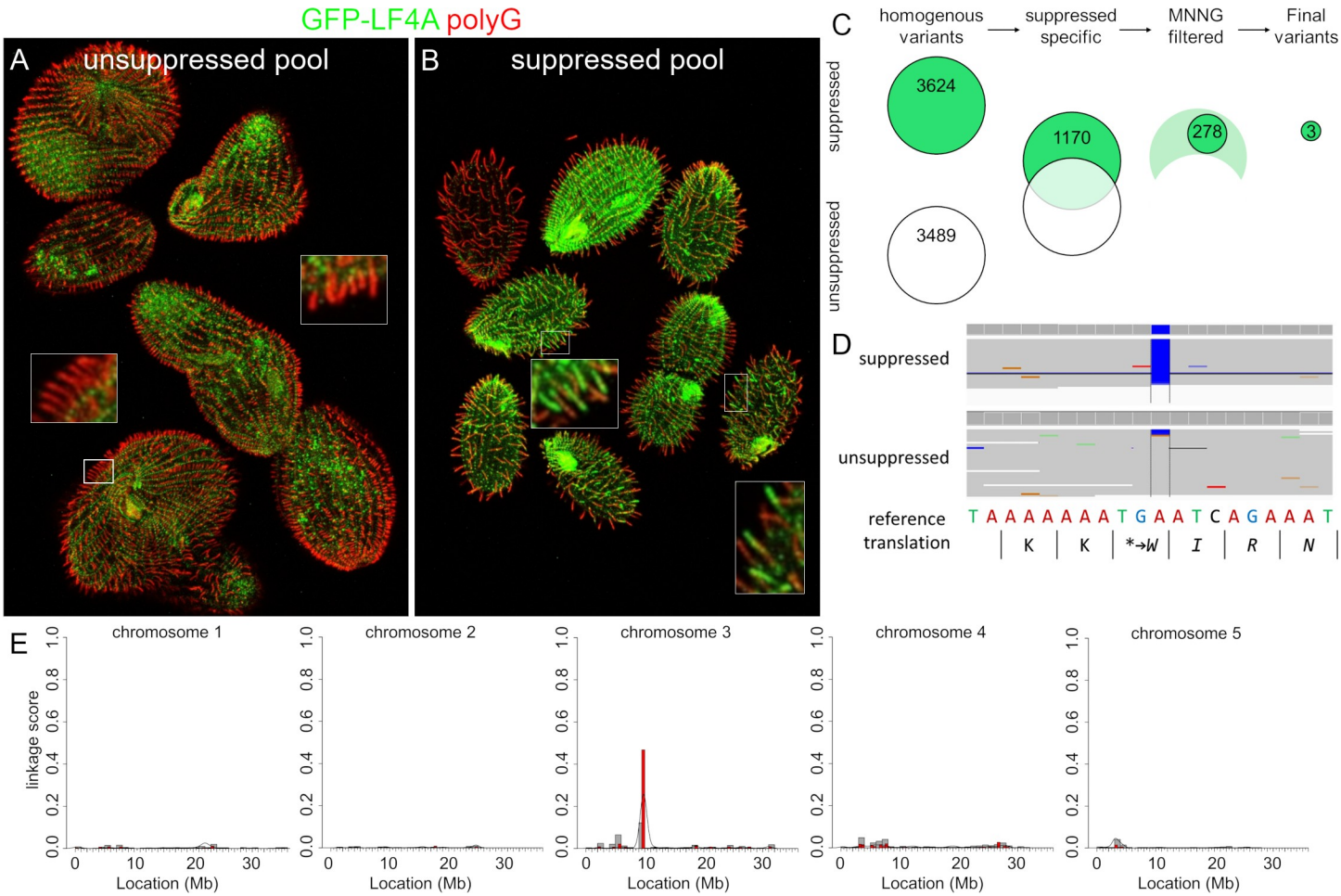


**Fig 5. The extragenic suppressor clone SUP1 has a mutation in *CDKR1*.** (A-B) Immunofluorescence images of (unsuppressed and suppressed) pools of F2 progeny derived from a single sup1/SUP1$^{+}$ (after an overnight exposure to $Cd^{2+}$) that were subsequently subjected to whole genome sequencing. Note the patterns of GFP-LF4A inside cilia: the base accumulation in the non-suppressed pool and the ciliary shaft and tip signals in the suppressed pool (see insets for higher magnifications). (C) The results of variant subtraction and filtering based on the alignment of sequencing reads to the macronuclear reference genome. Among the 278 variants consistent with nitrosoguanidine (MNNG) mutagenesis, three candidate variants affect a gene product and have a high fraction of reads supporting the alternative base in the mutant pool (see S1 Table). (D) An IGV browser view of the macronuclear genome sequence of *TTHERM_01080590* (*CDKR1*) that contains the variant scf_8254401:105680 T to C. This point mutation, supported by 100% of the sequencing reads from the mutant pool, changes the stop codon and adds a short peptide to the C-terminus of the predicted product. (E) An allelic composition contrast analysis of the variant co-segregation across all micronuclear chromosomes. The normalized linkage scores show the difference in the allelic composition between the mutant and the wild-type pool at each variant site. This reveals a cluster of variant co-segregation at 9–10 Mb on the micronuclear chromosome 3.

https://doi.org/10.1371/journal.pgen.1008099.g005

## CDKR1 is a negative regulator of cilium length that activates LF4A

In an otherwise wild-type background, the *cdkr1$^{sup1}$* allele mildly increased cilium length (Fig 4G). In cells overproducing GFP-LF4A, the *cdkr1$^{sup1}$* allele partially suppressed the shortening of cilia (Fig 4G). To clarify whether *cdkr1$^{sup1}$* is a gain or loss-of-function allele, we produced a strain with a null allele, CDKR1-KO. The locomotory cilia of CDKR1-KO cells were much longer than those of the wild-type or CDKR1$^{sup1}$ cells (Fig 6C compare with Figs 6A, 6E and 4G). Thus, likely the *cdkr1$^{sup1}$* allele is a hypomorph.

The CDKR1$^{sup1}$ protein has 10 extra amino acids at the C-terminus but is otherwise normal, and thus the effect of the sup1 mutation was unclear. We used homology modeling to predict the structure of CDKR1 and its sup1 version. The closest 3D structure available is the human CDK2 (PDBID: 2IW8) [87], to which we could align most of CDKR1 (I12-N308). We

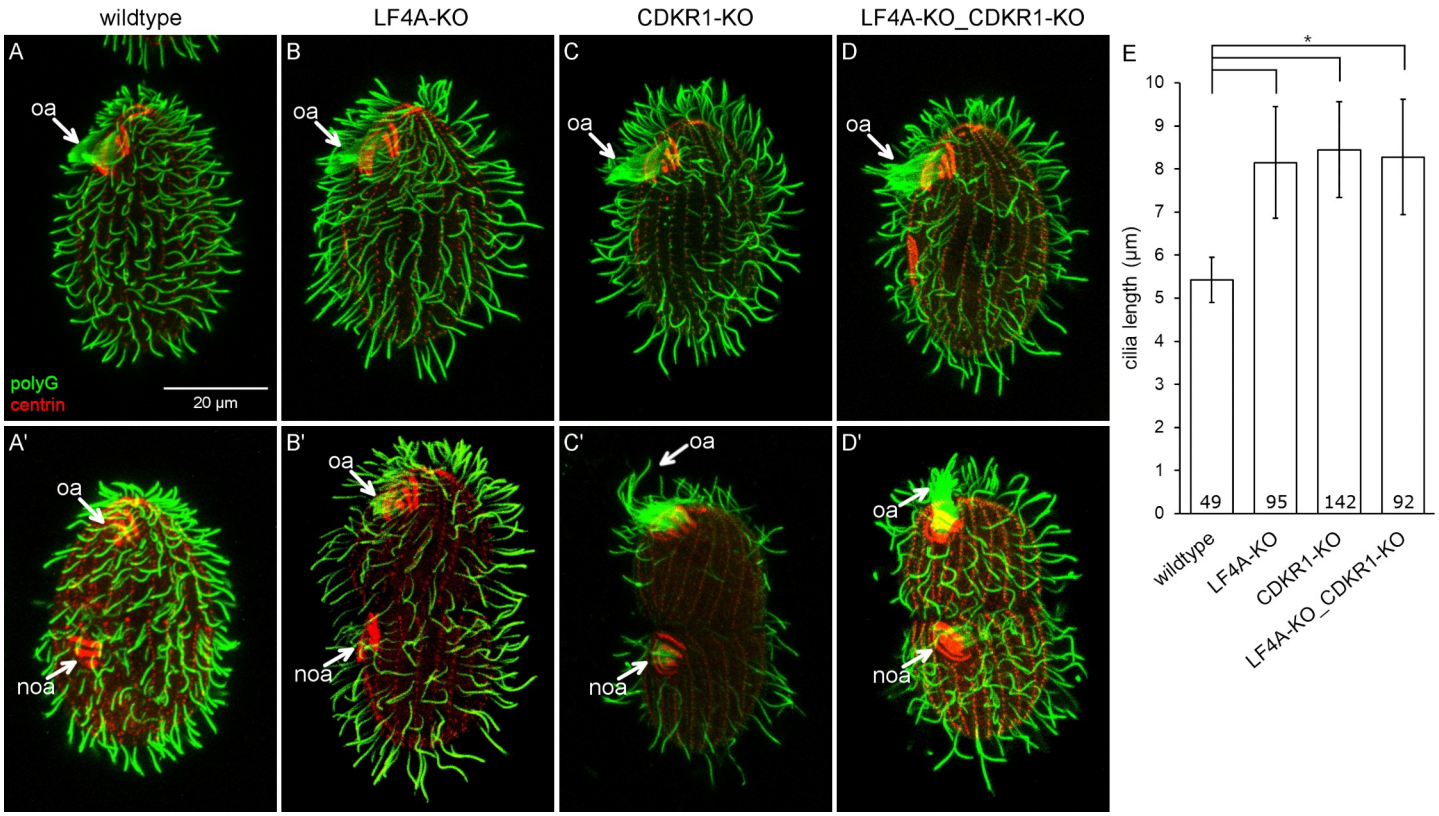


**Fig 6. A loss of CDKR1 lengthens both the locomotory and oral cilia.** (A-D') Wildtype (A and A'), LF4A-KO (B and B'), CDKR1-KO (C and C') and double knockout LF4A-KO_CDKR1-KO (D and D') cells that are either in interphase (top panels) or dividing (bottom panels). The cells were stained with the anti-polyG tubulin (green) and anti-centrin antibodies (red). (E) The locomotory cilia lengths in different backgrounds. The cilia length in LF4A-KO, CDKR1-KO and the double knockout strain are similar ($p > 0.01$) and all are significantly longer than the wild-type cilia (one way Anova, $p < 0.01$). Sample sizes are indicated, error bars indicate SDs.

https://doi.org/10.1371/journal.pgen.1008099.g006

attempted to model the remaining 23 (33 in sup1) C-terminal amino acids without a template. A Jpred [88] secondary structure prediction indicated that the LKKWIRNLL peptide in sup1 protein forms an alpha-helix. Thus, the WIRNLLILNG extension may enlarge the contact between the C-terminal tail of CDKR1 (that lies on the surface of the kinase domain) and the catalytically important C-helix (S5A Fig). As mentioned earlier, unlike the canonical CDKs that regulate the cell cycle, CDKR1 (and other cilia-associated CDK-related kinases DYF-18, LF2 and CCRK) lacks the cyclin-binding motif, PSTAIRE (S5C Fig). The WIRNLLILNG extension may pack to the region of the C-helix where cyclin typically binds in the canonical CDKs (S5B Fig). Thus, the C-terminal tail extension in the sup1 version may affect the C-helix conformation in the critical regulatory region that is important for kinase activation.

To explore further how CDKR1 may interact with LF4A, we compared the phenotypes of the respective null mutants. The locomotory cilia of CDKR1-KO cells were similar in length to those of LF4A-KO, and also more sparsely present in the posterior cell region (Fig 6A–6C and 6E). Strikingly, while the oral cilia seemed unaffected in LF4A-KO, they were exceptionally long in CDKR1-KO (Fig 6C compare to Fig 6A and 6B, marked with "oa"). The excessively long oral cilia were most striking in the old (anterior) oral apparatus of the dividing cells (Fig 6C' compare to Fig 6A' and 6B', the old oral apparatus marked with "oa") Unlike the wild-type and LF4A-KO cells, the CDKR1-KO cells could be maintained long-term only on the specialized medium MEPP that supports proliferation of mutants deficient in phagocytosis [89], indicating that the oral cilia in CDKR1-KO were functionally compromised. Overall the

phenotype of CDKR1-KO was more severe as compared to LF4A-KO. The two null alleles similarly affected the locomotory cilia but only the loss of CDKR1 lengthened the oral cilia. The double knockout (LF4A-KO_CDKR1-KO) cells had the phenotype similar to the single knockout CDKR1-KO, including long oral cilia (Fig 6D, 6D' and 6E). To summarize, both LF4A and CDKR1 regulate the length of locomotory cilia (likely by acting in the same linear pathway, see below), while only CDKR1 significantly contributes to the length of oral cilia.

Next, we examined how the phenotype of overexpression of GFP-LF4A (shortening of cilia) is affected by a complete loss of CDKR1. We compared two strains with the ovGFP-LF4A transgene that were either otherwise wild-type (CDKR1$^{+}$) or CDKR1-KO. Without $Cd^{2+}$ treatment, the ovGFP-LF4A_CDKR1$^{+}$ cells had normal length cilia, while the ovGFP-LF4A_CDKR1-KO cells had fewer and excessively long locomotory and oral cilia, as expected (Fig 7A and 7B). When GFP-LF4A overexpression was induced with $Cd^{2+}$, cilia shortened in both strains, but to a different degree. While ovGFP-LF4A_CDKR1$^{+}$ cells experienced a strong shortening of all cilia (locomotory and oral) (Fig 7C), in the ovGFP-LF4A_CDKR1-KO cells, both the locomotory and oral cilia shortened only partially and consequently had about a wild-type length (Fig 7D compare to Figs 7C and 1B). Next, we tested whether overproduction of GFP-LF4A in the CDKR1-KO background normalizes the functionality of cilia, by examining the cell multiplication rate, that in *Tetrahymena* is dependent on the health of both oral and locomotory cilia [65]. As expected, without added $Cd^{2+}$, the ovGFP-LF4A_CDKR1-KO cells grew more slowly than the ovGFP-LF4A_CDKR1$^{+}$ cells (Fig 7G). Remarkably, after addition of $Cd^{2+}$, the multiplication rate pattern had inverted; the ovGFP-LF4A_CDKR1$^{+}$ cells ceased to multiply, while the ovGFP-LF4A_CDKR1-KO cells multiplied faster (Fig 7G). Thus, a complete loss of CDKR1 is rescued by overexpression of LF4A. These observations argue that the major if not only function of CDKR1 is to positively regulate the kind of activity provided by LF4A.

One way how a loss of CDKR1 may affect the outcome of overexpression of GFP-LF4A is by decreasing its stability. Among three ovGFP-LF4A_CDKR1-KO clones (all derived from the same F1) that were phenotypically similar, the levels of overexpressed GFP-LF4A were highly variable (S6A Fig). Similarly, the levels of overproduced GFP-LF4A varied among several clones that all carried the *cdkr1*$^{sup1}$ allele (S6B Fig). While the sources of this variability are unclear, it appears that the suppression phenotype does not correlate with the levels of overproduced GFP-LF4A. Strikingly, GFP-LF4A overproduced in the CDKR1-KO cells, strongly accumulated near the tips of cilia (Fig 7F compare to Fig 7E), which is a phenocopy of the kinase-weak GFP-LF4A$^{F82A}$ (Figs 3C and S4C–S4E). Also, GFP-LF4 was enriched at the tips of some cilia in the presence of the hypomorphic allele *cdkr1*$^{sup1}$ but not in the wild-type background (Fig 4F compare to Fig 4D). These observations suggest that deficiencies of CDKR1 reduce the kinase activity of overproduced GFP-LF4A. Indeed, overproduced GFP-LF4A pulled down from either the CDKR1-KO or cdkr1$^{sup1}$ cells had reduced kinase activity *in vitro* as compared to the same protein from a wild-type background (Figs 7H and S6C). Thus, CDKR1 increases the kinase activity of LF4A. However, even without CDKR1, overproduced LF4A has residual kinase activity *in vitro* (Fig 7H) and *in vivo* as it partially shortens cilia (Fig 7D compare to Fig 7B).

Under the native conditions, CDKR1 regulates the length of locomotory cilia, most likely by activating LF4A (based on the similarity of the null phenotypes in regard to the locomotory cilia, Fig 6). To regulate the length of oral cilia, CDKR1 may activate LF4A and one or more of the seven unstudied RCKs (Fig 1A) that could be partially redundant with LF4A. That LF4A functions in both locomotory and oral cilia (despite a lack of effect of its loss on the length of oral cilia) is indicated by the presence of LF4A-GFP near the basal bodies (Fig 2B and 2C), the cilia-shortening activity of GFP-LF4A (Fig 3B) and the enrichment of multiple kinase-weak variants of GFP-LF4A at the tips (Figs 3C and S4C–S4E) of both locomotory and oral cilia. To

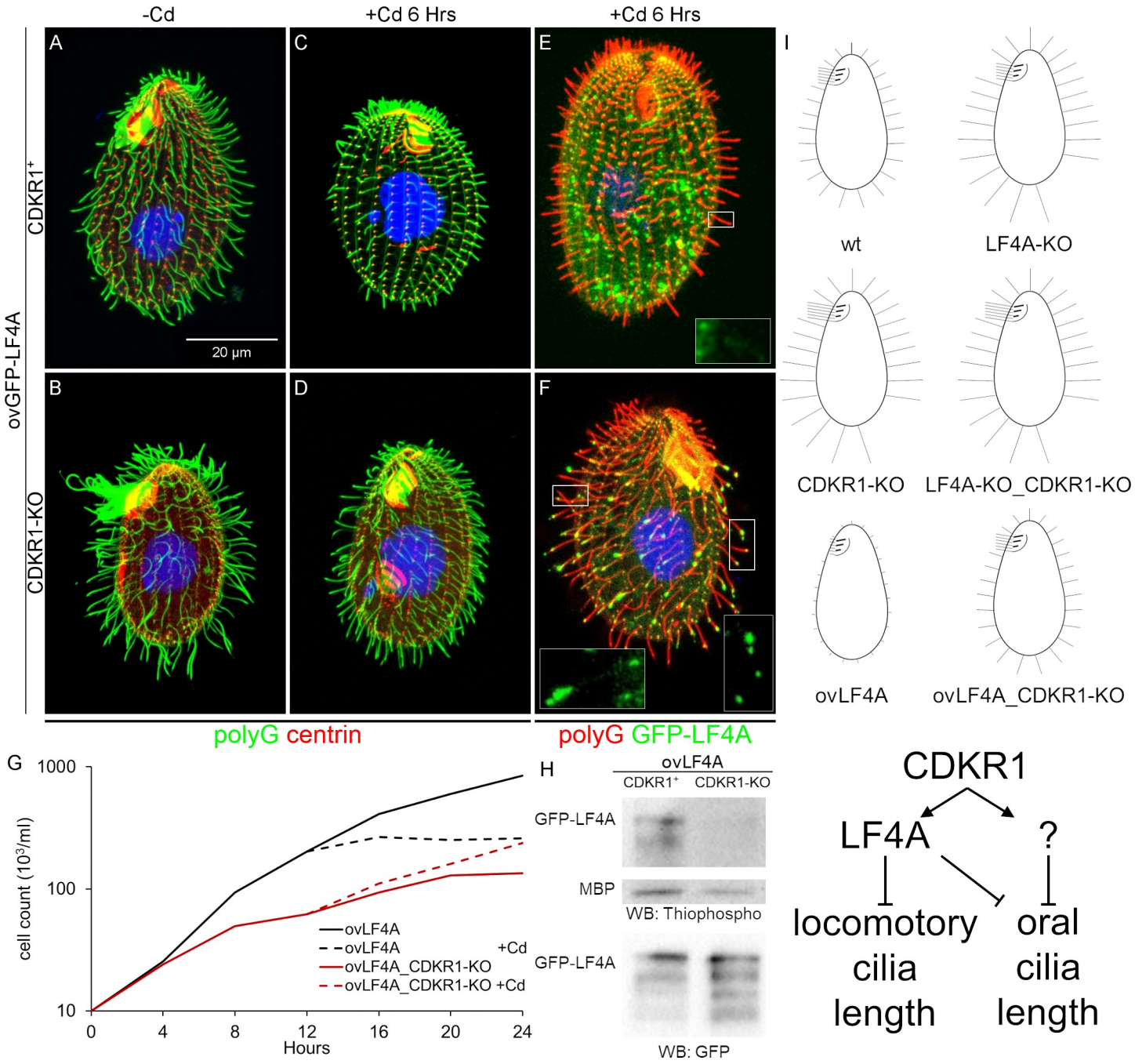


**Fig 7. A complete loss of CDKR1 rescues the cilia shortening induced by GFP-LF4A overexpression and reduces the LF4A kinase activity.** GFP-overproducing cells that have either wild-type CDKR1 (A, C, E) or are CDKR1-KO (B, D, F), imaged before (A and B) or after a 6 hours exposure to $Cd^{2+}$ (C, D, E and F). In A-D, the cells were stained with the anti-polyG antibodies (green) and anti-centrin antibodies (red). In (E) and (F), the cells show a GFP-LF4A signal (green) and are stained with anti-polyG antibodies (red). In cells lacking CDKR1, overproduced GFP-LF4A accumulated at the distal ends of cilia (F), indicating a reduced LF4A kinase activity. (G) The growth rates of multiple strains that overproduce GFP-LF4A and are either wild-type or CDKR1-KO. The cells were inoculated in SPPA media without $Cd^{2+}$ (each data point averages 6 cultures), and an overexpression of GFP-LF4A was induced at 12 hours (each data point averages 3 cultures hereafter). (H) An *in vitro* kinase activity of overproduced GFP-LF4A isolated from two strains that are either wild-type ($CDKR1^{+}$) or CDKR1-KO. The phosphorylated products were detected on a western blot probed with the anti-thiophosphorylation antibody 51–8 (the upper and middle panels show areas of the same blot containing the autophosphorylated GFP-LF4A and MBP, respectively). The same amounts of IP inputs were analyzed on a western blot probed with the anti-GFP antibodies shown in the bottom panel (WB: GFP) the multiple bands likely are proteolytic degradation products of GFP-LF4A. (I) Top: a graphical summary of the phenotypes and genotypes. Bottom: a scheme of the likely pathway involving CDKR1, LF4A and another kinase, likely an RCK that acts downstream of CDKR1 in oral cilia.

https://doi.org/10.1371/journal.pgen.1008099.g007

summarize, CDKR1 increases the kinase activity of LF4A to promote shortening of locomotory cilia and may act through LF4A and another RCK to shorten the oral cilia (Fig 7I).

## Discussion

### Ciliary and non-ciliary roles of RCKs

LF4/MOK and DYF-5/MAK/ICK are two subgroups of RCK kinases. While most ciliated lineages have both LF4/MOK and DYF-5/MAK/ICK, *C. elegans*, *Drosophila* and zebrafish lack LF4/MOK (Fig 1A); thus DYF-5/MAK/ICK can be sufficient for ciliary functions, suggesting that the two subtypes of RCKs have closely-related activities. While most RCKs have been linked to cilia, some non-ciliated species, including *Dictyostelium discoideum* and fungi, have RCKs (Fig 1A). In the budding yeast its RCK, Ime2, functions in meiosis and sporulation (reviewed in [90]). Among the two LF4/MOK homologs of *Tetrahymena*, LF4A regulates cilia, while LF4B is expressed during conjugation. Possibly, following the whole genome duplication [91], LF4A retained the ancestral ciliary function [92], while LF4B underwent neofunctionalization.

### RCKs and their CDK activators affect both cilium length and number

The *Tetrahymena* cells lacking either LF4A or its activator, CDKR1, have longer but also fewer locomotory cilia in the posterior dorsal region. In the mouse, a loss of ICK or its activator CCRK, in different cell types leads to either longer or shorter cilia [5, 42, 93]. In *Chlamydomonas*, hypomorphic LF2 alleles confer longer cilia, but a null allele produces variable length (including shorter) cilia and inability to regenerate cilia after deciliation [47, 64, 94]. Losses of either RCKs or LF2/CCRK cause excessive accumulation of IFT materials in cilia [40–42, 47, 93, 95], which could create roadblocks that reduce IFT. In the multiciliated *Tetrahymena*, the excessively long cilia may deplete factors whose concentration is rate-limiting for ciliogenesis in other parts of the same cell. Thus, the long, short or even absent cilia could be parts of a single phenotypic spectrum caused by an underlying defect of excessive cilia assembly. However, we can not exclude a possibility that in *Tetrahymena*, LF4A plays a more direct role in ciliogenesis.

### RCKs reduce IFT

The key question is how LF4/MOK (and other RCKs) control cilium length. Our observations, together with the work by others indicate that LF4/MOK (and more broadly RCKs) act on cilium length by inhibiting IFT. We show that the LF4A activity reduces the velocities of IFT trains. However, in *Chlamydomonas* and mammalian cells, deficiencies in LF4/MOK did not change the IFT train velocities [38, 40, 96]. In mammalian cells, a depletion of ICK increases the rate of anterograde IFT and its overexpression reduces the rate of retrograde IFT, respectively [38]. On the other hand, in *C. elegans*, loss of DYF-5 reduces IFT speeds in both directions [41, 46]. Thus, the effects of RCKs on IFT velocities are inconsistent across different models. In *Chlamydomonas*, the anterograde IFT velocity increases as the growing cilium lengthens [34]. It is therefore possible that at least some changes in the IFT velocities caused by manipulations of RCKs in different models are secondary to changes in cilium length.

RCKs could be controlling cilium length primarily by reducing the frequency of IFT trains. We show that in *Tetrahymena*, loss of LF4A increases while its overexpression reduces the IFT frequencies, especially in the anterograde direction. In *Chlamydomonas* a loss of LF4 increases the amount of IFT motors entering cilia [35]. In multiple models, cilia deficient in RCKs have elevated levels of IFT proteins [40–42, 95]. In the absence of RCKs, excessive anterograde IFT may not be balanced by the retrograde IFT, leading to accumulation of IFT proteins in cilia.

Another parameter that may contribute to the assembly rate is the cargo occupancy on IFT trains, which is known to be higher in growing cilia as compared to the steady-state or disassembling cilia [16, 17, 36]. While to our knowledge, the effects of RCKs on the IFT cargo occupancy have not been studied, in *Chlamydomonas*, a loss of LF2, a CDK kinase that acts upstream of LF4 [39, 40, 47, 64], increases the frequency of IFT trains carrying tubulin [16].

Recent studies have linked cilium length kinases, including RCKs, to kinesin-2. In *C. elegans*, loss-of-function mutations in DYF-5, and its likely upstream activator DYF-18, rescue the short cilia phenotype caused an autoinhibitory mutation in OSM-3 kinesin-2, indicating that DYF-5 and DYF-18 inhibit OSM-3 [46]. *In vitro*, ICK phosphorylates the tail of murine kinesin-2 motor subunit, KIF3A, at T674. While, in mammalian cells cilia are only mildly affected by T674A substitutions, mutating multiple phosphorylatable amino acids in the tail of KIF3A reduces ciliogenesis in zebrafish [42]. To summarize, the cilium-shortening influences of RCKs may be mediated by phosphorylation and inhibition of kinesin-2 and the resulting reduction of anterograde IFT.

To our knowledge, we are first to image an RCK in live cells under near-native conditions. Strikingly, in the cilium, most of LF4A-GFP particles are stationary and scattered along the cilium length. A small subset of LF4A-GFP particles occasionally undergoes diffusion or moves with the IFT speeds as reported for overexpressed MOK and ICK in mammalian cells [38] and DYF-5 in *C. elegans* [41, 46]. LF4A may have a microtubule-binding ability, based on our observation that overproduced GFP-LF4A decorates non-ciliary microtubules. Furthermore, in *Chlamydomonas* most of the ciliary LF4 remains associated with the axoneme after detergent extraction [40]. An anchorage at the axoneme could concentrate LF4/MOK near the passing IFT trains. Furthermore, the total exposure of IFT components to LF4/MOK could be higher in a longer cilium. In this manner, an increased axoneme length may be translated into a proportionally decreased IFT activity, which could contribute to the balance between the rate of assembly and the rate of disassembly at steady state. As argued above, the activity of LF4/MOK decreases the IFT train entry rate. Because IFT trains enter at the ciliary base, a component of IFT trains would need to be reused in the subsequent IFT round, to convey a length-dependent feedback of the axoneme-anchored LF4/MOK. While many of the IFT components are replaced by fresh IFT proteins that arrive from the cell body, some (including IFT54) are partially recycled [97].

On the other hand, there are indications that length-sensing is at least partly operational in the absence of LF4/MOK. Namely, in both the wild-type and LF4A-deficient *Tetrahymena*, the rate of assembly decelerates as the growing cilia approach their steady-state lengths (Fig 1E). Also, in *Chlamydomonas*, the rate of entry of kinesin-2 motors remains inversely proportional to cilium length in the absence of LF4 [35]. One possibility is that without LF4/MOK, the length-sensing feedback machinery utilizes other RCKs and the disassembly pathway, whose activity is known to be length-dependent [37]. Alternatively, LF4/MOK may act solely by reducing the rate of cilium assembly, without participating in the length-sensing activities. Under this scenario, the uniform distribution of LF4/MOK along cilium length may deliver a consistent dose of LF4/MOK-mediated inhibition of IFT from the cilium base to the distal tip.

## CDK-related kinases (LF2/CCRK and DYF-18/CDKR1) are activators of RCKs

The first evidence that CDK-related LF2/CCRK kinases acts upstream of RCKs was an observation in *Chlamydomonas*, that an LF2 mutation is epistatic to an LF4 mutation [39]. The mammalian ortholog of LF2, CCRK, phosphorylates ICK and MAK on threonine of the TxY motif in the kinase activation loop [98–101]. In glioblastoma cells, overexpression of ICK reduces ciliogenesis and this effect is suppressed by either a CCRK knockdown or by mutating

T157 in the TxY motif of ICK [43]. A recent study found that in *Chlamydomonas* LF4 is phosphorylated at T159 of the TxY motif, and this phosphorylation requires LF2, suggesting that LF2 phosphorylates T159 of LF4 [40]. Here we used an unbiased approach to identify a CDK-related protein, CDKR1, as an activator of LF4A. CDKR1 closely resembles LF2/CCRK and DYF-18. All these cilia-length regulating kinases are structurally similar to the canonical CDKs but lack the PSTAIRE cyclin-binding motif (S5C Fig). By analogy to other cilia-associated CDK kinases, CDKR1 may activate LF4A by phosphorylating the threonine in the TxY motif. Fu and colleagues showed that ICK is also weakly activated by autophosphorylation of tyrosine in the TxY motif [99]. Consistently, we show that LF4A is weakly active even without CDKR1 *in vitro* and *in vivo*. That overproduced LF4A rescues the cilia defects caused by a loss of CDKR1 indicates that the major function of CDKR1 is to activate LF4A or a similar activity provided by another kinase. Likely, CDKR1 acts by activating LF4A in the locomotory cilia and as discussed above, in addition to LF4A, activates another RCK in oral cilia. Our observations suggest that multiple RCKs are differentially utilized in different types of cilia and perhaps also among cilia located at different positions. Future studies on the seven uncharacterized DYF-5/ICK/MAK kinases of *Tetrahymena* could provide insights into how subsets of cilia are selectively managed by multiple length-regulating kinases in a single cell.

## Materials and methods

### Phylogenetic analysis of cilium length kinases

The cilium length-associated and CDK members of the CMGC kinase group were identified in multiple species by reciprocal BLASTp searches using sequences of well-studied CMGC members. Sequences were aligned with ClustalX 1.82 [102] and corrected manually in SEAVIEW [103]. A neighbor-joining tree was calculated with the Phylip package [104]. The tree was visualized using FIGTREE (http://tree.bio.ed.ac.uk/software/figtree/). The following are NCBI accession numbers, names and abbreviated names (used for the alignments and the phylogenetic tree): XP_001030514.2 (TTHERM_01080590, CDKR1), NP_503323.2 (DYF-18_Ce), NP_002737.2 (MAPK3_Hs), XP_001018592.1 (TTHERM_00286770), EAR97232.2 (TTHERM_00483640), XP_001020875.2 (TTHERM_00411810), NP_524420.1 (CDK2_Dm), XP_001027728.1 (TTHERM_01035490), XP_0010219111.2 (TTHERM_01207660), NP_001777.1 (CDK1_Hs), NP_009718.3 (CDC28_Sc), XP_001698637.1 (CDK_Cr), AAF55917.1 (CG6800_Dm), ABK34487.1 (LF2_Cr), NP_001034892.1 (CCRK_Hs), XP_009302023.1 (CDK20_Dr), NP_490952.2 (CDK7_Ce), NP_001790.1 (CDK7_Hs), NP_001256291.1 (CDKL5_Ce), NP_001124243.1 (CDKL5_Dr), NP_001310218.1 (CDKL5_Hs), XP_001008848.2 (TTHERM_00185770), AGC12987.1 (LF5_Cr), EAR90584.2 (TTHERM_00122330), EAR90792.3 (TTHERM_00141000), NP_055041.1 (MOK_Hs), AAO86687.1 (LF4_Cr), EAR83896.4 (TTHERM_00822360, LF4B), EAR87368.2 (TTHERM_00058800, LF4A), EAR93150.1 (TTHERM_00450990), EAR95676.2 (TTHERM_00267860), EAR89127.2 (TTHERM_00576780), EAR90889.2 (TTHERM_00144940), EAR82017.1 (TTHERM_01347900), XP_001697865.1 (MAPK7_Cr), NP_001129786.2 (Dyf-5_Ce), NP_001260307.1 (MAPK7_Dm), XP_009295564.1 (MAK_Dr), XP_011512721.1 (ICK_Hs), NP_005897.1 (MAK_Hs), XP_647537_Dd.

### Strains, culture and cilia regeneration

SPP medium [105] with antibiotics, SPPA [106] was used to grow *Tetrahymena* with exception of strains with severe cilia defects, which were maintained in MEPP medium [89] with 2 μg/ml dextrose (MEPPD) [25]. $CdCl_2$ (2.5 μg/ml) was added to the media to induce MTT1-driven overproduction of proteins [73]. Deciliation and cilia regeneration were done as described in [107].

## Gene disruption, native locus tagging and overexpression

**Native locus-based epitope tags.** To tag *LF4A* at the native locus, the plasmid pKIN13A-nativeGFP [25] was modified to make a derivative to target the 3' end of the *LF4A* coding region. To this end, 1.3 kb and 0.7 kb fragments of *LF4A* were amplified using the primer pairs: 5'-AATACCGCGGACTTTCAACCAAACAAAACTCA-3', 5'-TATTACGCGTTACTTATTAAAAACTGGCTTTTTACC-3' and 5'- AATAATCGATAAACTACTTTATAGCTGTTTGTTTTTGA-3', 5'-TTATGAGCTCGTGAGTCTAAACCTCCAGCAG-3' and cloned on the sides of a fragment consisting of a GFP coding region, a *BTU1* transcription terminator and a *neo3* cassette in reverse orientation.

To tag LF4B at the native locus, two 1.1 kb fragments were amplified using the primer pairs: 5'-ATAAGGGCCCGCAGCAGATGATAGTGGAG-3', 5'-TATTGAGCTCCATAGCATGGTACAGGAATCG-3', 5'-ATAACCGCGGTAAGTCTTTTTCAATGTTTATGC-3', 5'-TATTCTCGAGGAAAAAGGCTGGCAAGCG-3' and cloned on the sides of a fragment consisting of a GFP coding region, a *BTU1* transcription terminator and *neo5* in reverse orientation. The *neo5* cassette used is similar to the one published by others [108].

To engineer a plasmid for tagging IFT140 in the native locus, a 0.5 kb terminal fragment of a the *IFT140* coding region (TTHERM_00220810) was amplified using primers 5'-AATAACGCGTGTATTGAGTAATTAGAAACTAAGCTCAA-3' and 5'-AATTGGATCCTTCTGGGACATCTTCTTCAATG-3' and used to replace the corresponding part of pFAP43-GFP-neo4 [109] plasmid using MluI and BamHI sites. Next, a 0.9 kb fragment of the 3' UTR of *IFT140* was amplified using primers 5'-AAATCTGCAGCTTCATAGTAACTGACTACATTTAAAA-3' and 5'-AATTCTCGAGACAAGCCATGCGAAAATG-3' and cloned into pFAP43-GFP-neo4 using PstI and XhoI sites. Next *neo4* was replaced by the *pac* cassette that confers resistance to puromycin [110]. The resulted plasmid pIFT140-GFP-pac enables native expression of IFT140 with a C-terminal GFP tag separated from IFT140 by a short linker (GSGGGSGTG).

**Gene knockouts.** For disruption of *LF4A*, two 1.2 kb genomic fragments of *LF4A* were amplified using the primer pairs: 5'-TATTGGGCCCTAATTTTATGTGATAGTCTTTATG-3', 5'-TTATCCCGGGTGATTATCTCTAAATATTAATGTC-3', and 5'-TTAACTGCAGCAGATATATATGGGATAATATTTA-3', 5'-ATATCCGCGGTTTAGGAGTATATTTTCATAGTAT-3' and cloned on the sides of *neo4* [111]. The germline-based total homozygotes were tested for the absence of the targeted *LF4A* fragment using a diagnostic PCR with primers: 5'-GTTTCGCCTCATCCTCACAT-3' and 5'-AGAGAGATAATATGCAGGGCG-3'.

To disrupt *CDKR1*, the targeting homology arms were amplified with the following primer pairs: 5'-TATTGAGCTCAAATTTGAGGCACTACATTC-3', 5'-TATTCCGCGGATTACCAAGCAAATCAG-3' and 5'-TATTAAGCTTCATAAGCAAAAATAAAATGCC-3', 5'-TATTATCGATGTAAAACTGAGAGCATTTGC-3' and cloned on the sides of *neo5*. The loss of the targeted part of *CDKR1* was confirmed in homozygotes using diagnostic primers: 5'-TTTAAAGATGACTCTGTACC-3' and 5'-CTGCAAGAGACTTGTATGC-3' that amplify the targeted sequence.

**Overexpression.** For overexpression of GFP-LF4A at the *BTU1* locus, a 2.7 kb *LF4A* coding sequence was amplified using primers: 5'-TATTACGCGTCATGAACTAATATAAATTG-3', 5'-TATTGGATCCTCATTACTTATTAAAAAC-3' and cloned into pMTT1-GFP [112]. For overexpression of the kinase-weak GFP-LF4A$^{F82A}$ variant, the pMTT1-GFP-LF4A plasmid was subjected to site-directed mutagenesis using the QuikChange Lightning kit (Agilent 210518) with the primers 5'-CAGGACGTTTGGCACTAGTGGCTGAATTGATGGATCAGAACC-3' and 5'-GGTTCTGATCCATCAATTCAGCCACTAGTGCCAAACGTCCTG-3'.

For overexpression of GFP-LF4A at the native (*LF4A*) locus, a 1.3 kb 5' UTR fragment of *LF4A* was amplified with primers: 5'-AATAGAGCTCATTAAGATCTCCTAACATGGAAT-

3', 5'-TATTCCGCGGCTTCTCTGAGTAGCTTCAAACAA-3'. Next, a 3.5 kb fragment of GFP-LF4A from pMTT1p-GFP-LF4A was amplified with primers: 5'-AATAGTCGACGATGAGTAAAGGAGAAGAACTTTT-3', 5'-TATTGGGCCCTCATTACTTATTAAAAACTGGC-3'. These fragments were cloned on the sides of *neo5* immediately followed by a *MTT1* promotor to make pNeo5_ovGFP-LF4A. The pNeo5_ovGFP-LF4A plasmid was used for generating a germline integrant in which the MTT1 gene promoter is placed in front of a coding region expressing GFP-LF4A (in the *LF4A* locus) and the derived heterokaryon was used in the suppressor screen (see below).

Our *neo5* was used to make plasmids for somatic disruptions of *LF4A* and overproduction of GFP-LF4A (pNeo5_ovGFP-LF4A) in the background of MTT1-GFP-DYF1 placed in the *BTU1* locus as described [113].

To overexpress mCherry-LF4A, the GFP coding region in pNeo5_ovGFP-LF4A was replaced with that of mCherry [114], which was amplified with primers: 5'-CTAAACTTAAAATAATGGCCAAGTCGACGGTTTCAAAAGGAGAAGAAG-3', 5'-GATAACAATTTATATTAGTTCATGACGCGTTTGTAAAGTTCATCCATACC-3' from pNeo4-mCherry. To overexpress mCherry-LF4A$^{F82A}$, the GFP-LF4A part of pNeo5_ovGFP-LF4A was replaced with two fragments that provide the sequence of mCherry-LF4A$^{F82A}$ using NEBuilder Hifi DNA Assembly. The point mutation was created at the junction between the two fragments, which were amplified with the following primer pairs: 5'-CTAAACTTAAAATAATGGCCAAGTCGACGGTTTCAAAAGGAGAAGAAG-3', 5-CAATTCAGCCACTAGTGCCAAACGTCCTGTAG-3', 5'- GCACTAGTGGCTGAATTGATGGATCAGAACC-3' AND 5'-CAAAAGCTGGGTACCGGGCCCATATGGGTGGCGTG-3' from pNeo5_ovmCherry-LF4.

The pNeo5_ovmCherry-LF4A and pNeo5_ovmCherry-LF4A-F82A plasmids were also used for overexpression in the background of either MTT1$_p$-GFP-DYF1 placed in the *BTU1* locus as described [113] or IFT140-GFP in its own locus using a somatic (macronuclear) approach.

## Somatic and germline transformation

All procedures for generating somatic and germline transformants and crosses were done as described [106, 107] with some changes. For the germline biolistic transformation, 100 μg of plasmid DNA was digested with restriction enzymes to release the targeting fragment, and used to coat gold particles (SeaShell S550d or Chempur 900040), which were then deposited onto seven microcarriers and fitted into the hepta adapter (Biorad). A biolistic shooting was performed 4 hours after mixing of CU428 and B2086 strains. The hepta adapter assembly was positioned on the third slot from the top inside PDS1000/He and the rapture disk had the value of 1800 psi. The conjugating cells were spread as a thin layer onto a 10-cm wide Petri dish containing a layer of Tris-Agar (10 mM Tris-HCl pH 7.4, 1.5% agar) and positioned at the bottom-most slot of PDS1000/He. To generate homokaryons, we either used the standard procedure based on two rounds of genomic exclusion or the short circuit genomic exclusion (SCGE) [115] with either B*VI or B*VII [83]. Specifically, the homokaryons for SUP1, CDKR1-KO, LF4A-KO_CDKR1-KO, ovGFP-LF4A and ovGFP-LF4A_CDKR1-KO were made using the SCGE. For genotyping the *cdkr1$^{sup1}$* allele its sequence introduced an MboI restriction site that was detected in the 1 kb PCR product (with primers 5'-TGGTGATTTTGGATCAGCT-3' and 5'-CTTGCTTTCCTCAAATAAAC-3').

## Confocal and TIRF microscopy

For immunofluorescence, cells were stained as described [113] using a simultaneous fixation (2% paraformaldehyde) and permeabilization (0.5% Triton X-100). To test for association with the cytoskeleton, cells were permeabilized with 0.5% Triton X-100 prior to fixation with

paraformaldehyde. The primary antibodies were: anti-GFP (1:100 Abcam ab6556), anti-centrin 20H5 (1:200, Millipore 04–1624), and anti-polyglycine serum 2302 (1:200, gift of Martin Gorovsky, University of Rochester). The secondary antibodies were purchased from Jackson ImmunoResearch. Images were taken using a Zeiss LSM 710 or LSM 880 confocal microscope (63x oil immersion, 1x or 1.5x digital zoom) and analyzed with Fiji-ImageJ software [116]. The total internal reflection fluorescence microscopy of *Tetrahymena* was done as described [76]. Images and video recordings were processed in Fiji-ImageJ [116].

## Western blots

Protein samples were separated on a 10% SDS-PAGE. The gels were either stained with blue silver [117], or proteins were transferred onto a PVDF membrane for western blotting. Primary antibodies used with western blots were: anti-GFP (Abcam ab6556 at 1:5000 or Rockland 600-401-215 at 1:1000), and the anti-thiophosphate ester 51–8 (1:2000–5000, Abcam ab92570). Colorimetric images of stained gels and luminescent images of western blots were recorded using ChemiDoc MP System and processed with Image Lab (Biorad).

## *In vitro* kinase assay

*Tetrahymena* cultures at $2x10^5$ /ml (30 ml) of strains expressing GFP-LF4A were treated with $CdCl_2$ (2.5 μg/ml) for 3–5 hours, cells were collected at 1700 rcf for 3 min and washed once with 10 mM Tris-HCl (pH 7.5). A lysis buffer (5 ml per 30 ml of $Cd^{2+}$ induced cells) was added that contained 0.5% NP-40, a phosphatase inhibitor cocktail (20 mM beta-glycerophosphoate, 1 mM sodium orthovanadate, 1 mM $Na_4P_2O_7$, 20 mM NaF) and 70 mM E64, in TBS (20 mM Tris-HCl pH 7.5, 150 mM NaCl). PMSF was added to 1 mM immediately before suspending the cell pellets. The mixtures were kept on ice and were pipetted vigorously every 10 minutes for 3 times. Then, the mixtures were spun at 20,000 rcf for 15 minutes. The supernatants were collected, diluted with 2 volumes of TBS so that the NP-40 concentration is below 0.2% for immunoprecipitation with GFP-Trap beads (agarose, ACT-CM-GFA0050, Allele Biotech). The GFP-Trap beads were added to the diluted lysate (10–15 μl resin per 30 ml of the starting culture). The mixtures were then incubated at 4˚C for 2 hr. The beads were pelleted at 2500 rcf for 2 min, washed with: TBS, TBS with 500 mM NaCl, and the kinase buffer (50 mM Tris-HCl pH 7.2, 100 mM NaCl, 10mM $MgCl_2$). A total of 30 μl of the kinase buffer with 1 mM DTT, 100 μM ATP-gamma-S (Biolog 88453-52-5) and phosphatase inhibitors cocktails were added to no more than 15 μl of the beads slurry along with 20 μg MBP (Active Motif 31314). The kinase assay mixtures were incubated for 30–120 minutes at 30˚C. The reactions were either stored overnight refrigerated or immediately terminated by addition of 2.5 mM PNBM (Abcam ab138910) followed by incubation for 2 hours at room temperature. The samples were then treated with the sample buffer and separated by SDS-PAGE. The thio-phosphorylation was detected using the anti-thiophosphate ester antibody 51–8 (1:2000–5000, rabbit, Abcam ab92570).

## Genetic screen for suppressors of GFP-LF4A overexpression

The neo5-$MTT1_p$-GFP-LF4a fragment was targeted to the *LF4A* locus in the micronucleus by biolistic transformation as described [106] using the hepta adapter as outlined above. The heterokaryon strain named ovGFP-LF4A-HE-3B (mic: neo5-ovGFP-lf4a/neo5-ovGFP-lf4a mac: wildtype, VII) was grown to $1x10^5$ cells/ml (40 ml total), and treated with 10 μg/ml of nitrosoguanidine (Sigma-Aldrich) for 3 hours at 30˚C. The mutagenized culture was subjected to starvation in Dryl's buffer [118] (1.7 mM sodium citrate, 1 mM $NaH_2P0_4$, 1 mM $Na_2HPO_4$ and 1.5 mM $CaCl_2$), overnight at 30˚C. The mutagenized cells were mixed with an equal volume

and number of starved B*VI and subjected to uniparental cytogamy [79]. Briefly, 5–6 hours after strain mixing, the conjugating cells were treated with 1.4% glucose for 45 minutes (by addition of an appropriate volume of 20% glucose) and diluted with 7–8 volumes of sterile water. The cells were spun down, suspended in 30 ml of SPPA and split into 5 ml samples, each kept in a 500 ml round media bottle (six total) at room temperature overnight to complete conjugation. SPPA (45 ml) was added to each bottle, followed by incubation at 30˚C for 3 hr. Paromomycin was added to the final concentration of 200 μg/ml to select the conjugation progeny. After 24–36 hours of selection at 30˚C, the pm-r cells were collected by centrifugation, each sample was suspended in fresh 40 ml SPPA with 2.5 μg/ml $CdCl_2$ and incubated in 50 ml conical centrifuge tubes in vertical positions overnight at room temperature. Due to the GFP-LF4A overproduction and the resulting loss of cilia, unsuppressed cells become paralyzed and sunk to the bottom of the tubes. Cells carrying suppressor mutations remained motile near the tube top. The supernatants (4–5 ml) were collected from the top of each vertically positioned tube and the cells were transferred into 5 ml fresh SPPA in 15 ml conical tubes, incubated horizontally for 6 hours to overnight, then washed and suspended in 10 ml SPPA with 2.5 μg/ml $CdCl_2$ and the tubes were kept vertically oriented overnight. Single clones were isolated from the top 1 ml of culture of each tube and retested for suppression on 96-well plates. The F0s (isolated suppressor clones) were matured and mated to the cycloheximide resistance (cy-r) heterokaryon CU427 (mic: *chx1-1*/*chx1-1*, mac: + mt VI) or CU427.7 (mic: *chx1-1*/*chx1-1*, mac: + mt VII) and the F1 progeny was recovered as pm-r and cy-r cells. The F1s were matured and allowed to assort to paromomycin sensitivity (pm-s). To make F2s, assorted pm-s F1 were subjected to SCGE with B*VI or B*VII as described [83]. The F2s were cloned by picking pm-r cells from independently selected wells, grown in SPPA, and replica-plated on SPPA with 2.5 μg/ml $CdCl_2$ to test for paralysis.

## Identification of the causal mutations for suppressors

For the intragenic suppressors, total genomic DNA was extracted from a pool of F2s and the several 1–1.2 kb overlapping fragments covering MTT1p-ovGFP-LF4A transgene were amplified and sequenced using the Sanger method.

Pools of clones were prepared containing pm-r F2s obtained by SCGE from a single sup1/sup1$^+$ F1. The unsuppressed pool contained 12 F2s clones that consistently became paralyzed in $Cd^{2+}$ and the suppressed pool contained 14 F2 clones that remained motile in $Cd^{2+}$. The two pools were grown in 25 ml volumes, starved for 2 days at room temperature in 60 mM Tris-HCl and the total genomic DNAs of the pools were extracted, using the urea method [119]. The genomic DNAs were subjected to whole genome sequencing using Illumina technology exactly as described [83]. Sequences were aligned to the macronuclear reference genome (June 2014 version, GenBank assembly accession GCA_000189635.1) [120] and variants were detected filtered and subtracted as described [83]. In parallel, the suppressor and non-suppressor reads where aligned to the micronuclear reference genome [121] and the allelic contrast analysis was performed as described [83] to detect a micronuclear chromosome location with increased frequency of variant co-segregation with the mutant (suppressed) phenotype using MiModD (Version 0.1.8 [122]).

## Structural modeling of LF4A and CDKR1 kinases

Curated multiple sequence alignment profiles of protein kinases from diverse organisms were used to classify CDKR1 [68, 123, 124]. MAPGAPS [125] and HMMER [126] were used to detect and align CDKR1 to the best matching CDC2 profile [127].

The template for 3D homology modeling of LF4A was identified by performing a BLAST search against the PDB database using blastp routine from the NCBI [128]. The cyclin-dependent kinase from *Cryptosporidium* (Chain A of PDB 3NIZ, 37% sequence identity) was chosen as the template. MODELLER (version 9.12) was used to generate the homology model for LF4A from 3NIZ using the automodel module [81]. ADP and magnesium ions present in the template were also included in the modeled structure of LF4A. Jpred [88] was used to generate a secondary structure prediction of the CDKR1 (TTHERM_01080590) sequence. To make a structural model of CDKR1, *ab initio* protein structure prediction algorithms and I-TASSER were used [129–132]. The visualization of the modeled structures was performed using PyMOL [129].

## Supporting information

**S1 Fig. L4B is associated with the cell-cell junction during conjugation.** (A-C) Cells expressing LF4B-GFP (the tag added by engineering the native locus) analyzed by immunofluorescence using anti-GFP antibodies (red) 12G10 anti-α-tubulin (green only in panel C) and DAPI (Blue). (A) A vegetatively growing cell. Note an absence of a GFP signal above the typical background. (B-C) A conjugating pair. Note that LF4B-GFP localizes to the junction between the two mating cells. (D) Expression profiles of mRNAs for LF4A (TTHERM_00058800) and LF4B (TTHERM_00822360) obtained from the *Tetrahymena* Functional Genomics database (http://tfgd.ihb.ac.cn/search/detail/gene/TTHERM_00822360). The levels of mRNA at the following conditions are shown: L-l, L-m and L-h: vegetatively growing cells collected at ~$1x10^5$ cells/ml, ~$3.5x10^5$cells/ml and ~$1x10^6$ cells/ml. S-0, S-3, S-6, S-9, S-12, S-15 and S-24: cells starved for 0, 3, 6, 9, 12, 15 and 24 hours. C-0, C-2, C-4, C-6, C-8, C-10, C-12, C-14, C-16 and C-18: conjugating cells collected at 0, 2, 4, 6, 8, 10, 12, 14, 16 and 18 hours after initiation of conjugation by mixing different mating types.
(TIF)

**S2 Fig. Association of GFP-LF4A with microtubules and its co-transport with IFT.** (A) TIRF images of live cells overexpressing GFP-LF4A (left), kinase-weak GFP-$LF4A^{F82A}$ variant (middle), and kinase weak mCherry-$LF4A^{F82A}$. Overexpressed GFP-LF4A (right panel) localized to the bases of cilia and along cilia but also near the microtubule-rich structures in the cell body including longitudinal microtubules (lm), and contractile vacuole pores (cvp). The kinase-weak GFP-$LF4A^{F82A}$ is enriched at the tips of cilia while mCherry-$LF4A^{F82A}$ is distributed uniformly along cilia. (B) Kymographs that document co-migration of IFT proteins (GFP-DYF1 or IFT140-GFP, top) and either mCherry-LF4A or mCherry-LF4AF82A after induction with $Cd^{2+}$ (3 hours). (C) Signal intensity profiles of single cilia in cells expressing either mCherry-LF4 or mCherry-LF4F82A (red) and IFT140-GFP (green). The base is on the left and the tip is on the right side of each profile. Note that the active kinase is enriched at the base (left profile). The weak kinase is enriched at the base and spread along the cilium length when overproduced but does not accumulate at the tip. The pattern distribution of IFT140 is similar in all backgrounds and conditions, with enrichment at the tip.
(TIF)

**S3 Fig. A detailed presentation of the pipeline used for identifying suppressors of overexpression of GFP-LF4A.** (A) Steps involved in generation and isolation of the suppressor F0s. A heterokaryon with the ovGFP-LF4A transgene in the micronucleus (solid black) was subjected to mutagenesis with nitrosoguanidine. The mutagenized heterokaryon was subjected to a self-cross (uniparental cytogamy) that involves mating to a star strain that lacks a functional micronucleus. The outcome includes the desired self-cross progeny (uniparental cytogamonts,

typically a few % of the conjugated pairs), cells that failed to undergo conjugation (nonconjugants) and round one genomic exclusion, the most common outcome of such a cross (typically >95%). The uniparental cytogamy progeny were selected with paromomycin (pm) as they expressed the transgene in the macronucleus. The suppressor F0s were then isolated by collecting cells that remained mobile after overnight $Cd^{2+}$ exposure. (B) Steps used to determine whether the suppression is intragenic or extragenic. Each suppressor F0 clone underwent sexual maturation and was mated to CU427, a strain with a micronucleus carrying a homozygous *chx1-1* allele (resistance to cycloheximide cy) and a wild-type macronucleus. The outcross progeny was selected with cy and pm. F1 clones underwent phenotypic assortment to pm-s and become sexually mature. The pm-s F1 clone was then subjected to self-cross (short-circuit genomic exclusion) and the pm-r F2 clones were obtained. A number of F2 clones of each suppressor were tested for suppression by $Cd^{2+}$ treatment. An intragenic suppressor gives only suppressed F2 clones. An extragenic suppressor gives both unsuppressed (paralyzed) and suppressed F2 progeny.
(TIF)

**S4 Fig. Phenotypes of intragenic and extragenic suppressors of GFP-LF4A overexpression.** Self-cross progeny at a control background of GFP-LF4A overexpression (A), the extragenic suppressor SUP1 (B) and three intragenic suppressors SUP3, SUP4 and SUP5 (C-E). All cells were subjected to a 6-hours $Cd^{2+}$ exposure prior to immunofluorescence assay and showed the GFP signal (green) and were stained with anti-polyG antibodies (red).
(TIF)

**S5 Fig. A predicted structure suggests that the C-terminal tail extension in $CDKR1^{sup1}$ affects the kinase function.** (A) Predicted structure of $CDKR1^{sup1}$ with a C-terminal tail (with a WIRNLLILNG extension) forming two helical segments on the top of C-helix. (B) 3D view comparison of the C-helix (and cyclin-CDK interface) of $CDKR1^{sup1}$ and a CDK2. A PSTAIRE sequence in the canonical CDKs lies at the interface of the cyclin-CDK complex and corresponds to the C-helix in the CDKs. The equivalent positions in CDKR1 are KQIVERE. (C) A sequence alignment of fragments of CDK and CDK-related kinases.
(TIF)

**S6 Fig. A loss of CDKR1 does not consistently affects the levels of overproduced GFP-LF4A.** (A) A comparison of the levels of GFP-LF4A in whole cell lysates of several F2 clones derived from the same F1, with or without a 6-hour $Cd^{2+}$ exposure. An ovGFP-LF4A_$CDKR1^{+}$ control strain and three ovGFP-LF4A_CDKR1-KO F2s were analyzed. (B) A comparison of the levels of GFP-LF4A in whole cell lysates of the F2 progeny clones of the extragenic suppressor SUP1, with or without a 6-hour $Cd^{2+}$ exposure. An unsuppressed (ovGFP-LF4A_$CDKR1^{+}$) strain and four suppressed (ovGFP-LF4A_$CDKR1^{sup1}$) strains were analyzed. Faster-migrating bands represent degradation products of GFP-LF4A. (C) In vitro kinase assays show that loss-of-function of CDKR1 results in a reduced kinase activity of overproduced GFP-LF4A against itself and MBP. The top panel is a western blot that reveals the signal of thiophosphorylated substrates. The bottom panel is a western blot that documents the levels of GFP-LF4A in the reactions using anti-GFP antibodies.
(TIF)

**S1 Video. A live cell expressing LF4A-GFP (under the native promoter) recorded by TIRFM.** The frame rate is 3 times of the real time. Examples of rare cilia with mobile LF4A-GFP are marked by red boxes.
(MOV)

**S2 Video. A TIRFM video of a live wild-type cell expressing GFP-DYF1 reporter (treated with Cd2+ for 3.5 hours).** The frame rate is 3 times of the real time.
(MP4)

**S3 Video. A TIRFM video of a live cell that overexpresses GFP-LF4A (treated with Cd2 + for 3.5 hours) and also expresses GFP-DYF1 reporter.** The frame rate is 3 times of the real time.
(MP4)

**S1 Table. The candidate causal variants identified in the SUP1 suppressor genome based on bioinformatic subtractions and filtering.**
(XLSX)

## Acknowledgments

We thank Martin A. Gorovsky (University of Rochester) for the polyG antibodies. We also acknowledge the assistance of Muthugapatti K. Kandasamy at the UGA Biomedical Microscopy Core with confocal imaging.

## Author Contributions

**Conceptualization:** Yu-Yang Jiang, Jacek Gaertig.

**Funding acquisition:** Ralf Baumeister, Dorota Wloga, Natarajan Kannan, Jacek Gaertig.

**Investigation:** Yu-Yang Jiang, Wolfgang Maier, Ewa Joachimiak, Dorota Wloga, Zheng Ruan, Stephen Bocarro, Anoosh Bahraini, Krishna Kumar Vasudevan.

**Methodology:** Yu-Yang Jiang, Wolfgang Maier, Gregory Minevich, Eduardo Orias, Jacek Gaertig.

**Project administration:** Jacek Gaertig.

**Resources:** Karl Lechtreck.

**Supervision:** Ralf Baumeister, Dorota Wloga, Natarajan Kannan, Karl Lechtreck, Jacek Gaertig.

**Writing – original draft:** Yu-Yang Jiang, Jacek Gaertig.

**Writing – review & editing:** Yu-Yang Jiang, Wolfgang Maier, Ralf Baumeister, Gregory Minevich, Ewa Joachimiak, Dorota Wloga, Zheng Ruan, Karl Lechtreck, Eduardo Orias, Jacek Gaertig.

## References

1. Rosenbaum JL, Moulder JE, Ringo DL. Flagellar elongation and shortening in *Chlamydomonas*. The use of cycloheximide and colchicine to study the sythesis and assembly of flagellar proteins. JCell Biol. 1969; 41:600–19.
2. Dafinger C, Liebau MC, Elsayed SM, Hellenbroich Y, Boltshauser E, Korenke GC, et al. Mutations in KIF7 link Joubert syndrome with Sonic Hedgehog signaling and microtubule dynamics. J Clin Invest. 2011; 121(7):2662–7. Epub 2011/06/03. https://doi.org/10.1172/JCI43639 PMID: 21633164; PubMed Central PMCID: PMC3223820.
3. Tammachote R, Hommerding CJ, Sinders RM, Miller CA, Czarnecki PG, Leightner AC, et al. Ciliary and centrosomal defects associated with mutation and depletion of the Meckel syndrome genes MKS1 and MKS3. Hum Mol Genet. 2009; 18(17):3311–23. Epub 2009/06/12. https://doi.org/10.1093/hmg/ddp272 PMID: 19515853; PubMed Central PMCID: PMC2733821.

4. Slaats GG, Isabella CR, Kroes HY, Dempsey JC, Gremmels H, Monroe GR, et al. MKS1 regulates ciliary INPP5E levels in Joubert syndrome. J Med Genet. 2016; 53(1):62–72. Epub 2015/10/23. https://doi.org/10.1136/jmedgenet-2015-103250 PMID: 26490104; PubMed Central PMCID: PMC5060087.
5. Moon H, Song J, Shin JO, Lee H, Kim HK, Eggenschwiller JT, et al. Intestinal cell kinase, a protein associated with endocrine-cerebro-osteodysplasia syndrome, is a key regulator of cilia length and Hedgehog signaling. Proc Natl Acad Sci U S A. 2014; 111(23):8541–6. https://doi.org/10.1073/pnas.1323161111 PMID: 24853502; PubMed Central PMCID: PMC4060650.
6. Oud MM, Bonnard C, Mans DA, Altunoglu U, Tohari S, Ng AY, et al. A novel ICK mutation causes ciliary disruption and lethal endocrine-cerebro-osteodysplasia syndrome. Cilia. 2016; 5:8. https://doi.org/10.1186/s13630-016-0029-1 PMID: 27069622; PubMed Central PMCID: PMC4827216.
7. Thiel C, Kessler K, Giessl A, Dimmler A, Shalev SA, von der Haar S, et al. NEK1 mutations cause short-rib polydactyly syndrome type majewski. Am J Hum Genet. 2011; 88(1):106–14. Epub 2011/01/08. https://doi.org/10.1016/j.ajhg.2010.12.004 PMID: 21211617; PubMed Central PMCID: PMC3014367.
8. Taylor SP, Dantas TJ, Duran I, Wu S, Lachman RS, University of Washington Center for Mendelian Genomics C, et al. Mutations in DYNC2LI1 disrupt cilia function and cause short rib polydactyly syndrome. Nature communications. 2015; 6:7092. Epub 2015/06/17. https://doi.org/10.1038/ncomms8092 PMID: 26077881; PubMed Central PMCID: PMC4470332.
9. Stone EM, Luo X, Heon E, Lam BL, Weleber RG, Halder JA, et al. Autosomal recessive retinitis pigmentosa caused by mutations in the MAK gene. Investigative ophthalmology & visual science. 2011; 52(13):9665–73. Epub 2011/11/24. https://doi.org/10.1167/iovs.11-8527 PMID: 22110072; PubMed Central PMCID: PMC3341124.
10. Ozgul RK, Siemiatkowska AM, Yucel D, Myers CA, Collin RW, Zonneveld MN, et al. Exome sequencing and cis-regulatory mapping identify mutations in MAK, a gene encoding a regulator of ciliary length, as a cause of retinitis pigmentosa. Am J Hum Genet. 2011; 89(2):253–64. Epub 2011/08/13. https://doi.org/10.1016/j.ajhg.2011.07.005 PMID: 21835304; PubMed Central PMCID: PMC3155188.
11. Grati M, Chakchouk I, Ma Q, Bensaid M, Desmidt A, Turki N, et al. A missense mutation in DCDC2 causes human recessive deafness DFNB66, likely by interfering with sensory hair cell and supporting cell cilia length regulation. Hum Mol Genet. 2015; 24(9):2482–91. Epub 2015/01/21. https://doi.org/10.1093/hmg/ddv009 PMID: 25601850; PubMed Central PMCID: PMC4383862.
12. Liu S, Lu W, Obara T, Kuida S, Lehoczky J, Dewar K, et al. A defect in a novel Nek-family kinase causes cystic kidney disease in the mouse and in zebrafish. Development. 2002; 129(24):5839–46. https://doi.org/10.1242/dev.00173 PMID: 12421721.
13. Upadhya P, Birkenmeier EH, Birkenmeier CS, Barker JE. Mutations in a NIMA-related kinase gene, Nek1, cause pleiotropic effects including a progressive polycystic kidney disease in mice. Proc Natl Acad Sci U S A. 2000; 97(1):217–21. https://doi.org/10.1073/pnas.97.1.217 PMID: 10618398.
14. Castren M, Gaily E, Tengstrom C, Lahdetie J, Archer H, Ala-Mello S. Epilepsy caused by CDKL5 mutations. Eur J Paediatr Neurol. 2011; 15(1):65–9. https://doi.org/10.1016/j.ejpn.2010.04.005 PMID: 20493745.
15. Kozminski KG, Johnson KA, Forscher P, Rosenbaum JL. A motility in the eukaryotic flagellum unrelated to flagellar beating. Proc Natl Acad Sci USA. 1993; 90:5519–23. https://doi.org/10.1073/pnas.90.12.5519 PMID: 8516294
16. Craft JM, Harris JA, Hyman S, Kner P, Lechtreck KF. Tubulin transport by IFT is upregulated during ciliary growth by a cilium-autonomous mechanism. J Cell Biol. 2015; 208(2):223–37. https://doi.org/10.1083/jcb.201409036 PMID: 25583998; PubMed Central PMCID: PMC4298693.
17. Wren KN, Craft JM, Tritschler D, Schauer A, Patel DK, Smith EF, et al. A differential cargo-loading model of ciliary length regulation by IFT. Curr Biol. 2013; 23(24):2463–71. https://doi.org/10.1016/j.cub.2013.10.044 PMID: 24316207; PubMed Central PMCID: PMC3881561.
18. Qin H, Diener DR, Geimer S, Cole DG, Rosenbaum JL. Intraflagellar transport (IFT) cargo: IFT transports flagellar precursors to the tip and turnover products to the cell body. J Cell Biol. 2004; 164(2):255–66. Epub 2004/01/14. https://doi.org/10.1083/jcb.200308132 PMID: 14718520; PubMed Central PMCID: PMC2172340.
19. Cole DG, Diener DR, Himelblau AL, Beech PL, Fuster JC, Rosenbaum JL. Chlamydomonas kinesin-II-dependent intraflagellar transport (IFT): IFT particles contain proteins required for ciliary assembly in Caenorhabditis elegans sensory neurons. J Cell Biol. 1998; 18:993–1008.
20. Kozminski KG, Beech PL, Rosenbaum JL. The *Chlamydomonas* kinesin-like protein FLA10 is involved in motility associated with the flagellar membrane. J Cell Biol. 1995; 131:1517–27. https://doi.org/10.1083/jcb.131.6.1517 PMID: 8522608

21. Pazour GJ, Wilkerson CG, Witman GB. A dynein light chain is essential for the retrograde particle movement of intraflagellar transport (IFT). J Cell Biol. 1998; 141:979–92. https://doi.org/10.1083/jcb.141.4.979 PMID: 9585416

22. Signor D, Wedaman KP, Orozco JT, Dwyer ND, Bargmann CI, Rose LS, et al. Role of a class DHC1b dynein in retrograde trasnport of IFT motors and IFT raft particles along cilia but not dentrites, in chemosensory neurons of living Caenorhabditis elegans. JCellBiol. 1999; 147(3):519–30.

23. Porter ME, Bower R, Knott JA, Byrd P, Dentler W. Cytoplasmic dynein heavy chain 1b is required for flagellar assembly in Chlamydomonas. Mol Biol Cell. 1999; 10:693–712. https://doi.org/10.1091/mbc.10.3.693 PMID: 10069812

24. Niwa S, Nakajima K, Miki H, Minato Y, Wang D, Hirokawa N. KIF19A is a microtubule-depolymerizing kinesin for ciliary length control. Dev Cell. 2012; 23(6):1167–75. https://doi.org/10.1016/j.devcel.2012.10.016 PMID: 23168168.

25. Vasudevan KK, Jiang YY, Lechtreck KF, Kushida Y, Alford LM, Sale WS, et al. Kinesin-13 regulates the quantity and quality of tubulin inside cilia. Mol Biol Cell. 2015; 26(3):478–94. https://doi.org/10.1091/mbc.E14-09-1354 PMID: 25501369.

26. Piao T, Luo M, Wang L, Guo Y, Li D, Li P, et al. A microtubule depolymerizing kinesin functions during both flagellar disassembly and flagellar assembly in Chlamydomonas. Proc Natl Acad Sci U S A. 2009; 106(12):4713–8. Epub 2009/03/07. https://doi.org/10.1073/pnas.0808671106 PMID: 19264963; PubMed Central PMCID: PMC2660737.

27. Wang L, Piao T, Cao M, Qin T, Huang L, Deng H, et al. Flagellar regeneration requires cytoplasmic microtubule depolymerization and kinesin-13. J Cell Sci. 2013. Epub 2013/02/19. https://doi.org/10.1242/jcs.124255 PMID: 23418346.

28. Hu Z, Liang Y, Meng D, Wang L, Pan J. Microtubule-depolymerizing kinesins in the regulation of assembly, disassembly, and length of cilia and flagella. Int Rev Cell Mol Biol. 2015; 317:241–65. Epub 2015/05/27. https://doi.org/10.1016/bs.ircmb.2015.01.008 PMID: 26008787.

29. Kubo T, Hirono M, Aikawa T, Kamiya R, Witman GB. Reduced tubulin polyglutamylation suppresses flagellar shortness in Chlamydomonas. Mol Biol Cell. 2015; 26(15):2810–22. https://doi.org/10.1091/mbc.E15-03-0182 PMID: 26085508; PubMed Central PMCID: PMC4571340.

30. Huang K, Diener DR, Rosenbaum JL. The ubiquitin conjugation system is involved in the disassembly of cilia and flagella. J Cell Biol. 2009; 186(4):601–13. Epub 2009/08/26. https://doi.org/10.1083/jcb.200903066 PMID: 19704024; PubMed Central PMCID: PMC2733750.

31. Wang Q, Peng Z, Long H, Deng X, Huang K. Poly-ubiquitylation of alpha-tubulin at K304 is required for flagellar disassembly in Chlamydomonas. J Cell Sci. 2019. Epub 2019/02/16. https://doi.org/10.1242/jcs.229047 PMID: 30765466.

32. Liang Y, Meng D, Zhu B, Pan J. Mechanism of ciliary disassembly. Cellular and molecular life sciences: CMLS. 2016; 73(9):1787–802. https://doi.org/10.1007/s00018-016-2148-7 PMID: 26869233.

33. Marshall WF, Rosenbaum JL. Intraflagellar transport balances continuous turnover of outer doublet microtubules: implications for flagellar length control. J Cell Biol. 2001; 155(3):405–14. Epub 2001/10/31. https://doi.org/10.1083/jcb.200106141 PMID: 11684707; PubMed Central PMCID: PMC2150833.

34. Engel BD, Ludington WB, Marshall WF. Intraflagellar transport particle size scales inversely with flagellar length: revisiting the balance-point length control model. J Cell Biol. 2009; 187(1):81–9. Epub 2009/10/07. https://doi.org/10.1083/jcb.200812084 PMID: 19805630; PubMed Central PMCID: PMC2762100.

35. Ludington WB, Wemmer KA, Lechtreck KF, Witman GB, Marshall WF. Avalanche-like behavior in ciliary import. Proc Natl Acad Sci U S A. 2013; 110(10):3925–30. Epub 2013/02/23. https://doi.org/10.1073/pnas.1217354110 PMID: 23431147.

36. Pan J, Snell WJ. Chlamydomonas shortens its flagella by activating axonemal disassembly, stimulating IFT particle trafficking, and blocking anterograde cargo loading. Dev Cell. 2005; 9(3):431–8. https://doi.org/10.1016/j.devcel.2005.07.010 PMID: 16139231.

37. Hilton LK, Gunawardane K, Kim JW, Schwarz MC, Quarmby LM. The kinases LF4 and CNK2 control ciliary length by feedback regulation of assembly and disassembly rates. Curr Biol. 2013; 23(22):2208–14. https://doi.org/10.1016/j.cub.2013.09.038 PMID: 24184104.

38. Broekhuis JR, Verhey KJ, Jansen G. Regulation of cilium length and intraflagellar transport by the RCK-kinases ICK and MOK in renal epithelial cells. PLoS One. 2014; 9(9):e108470. https://doi.org/10.1371/journal.pone.0108470 PMID: 25243405; PubMed Central PMCID: PMC4171540.

39. Berman SA, Wilson NF, Haas NA, Lefebvre PA. A novel MAP kinase regulates flagellar length in Chlamydomonas. Curr Biol. 2003; 13(13):1145–9. Epub 2003/07/05. PMID: 12842015.

40. Wang Y, Ren Y, Pan J. Regulation of flagellar assembly and length in Chlamydomonas by LF4, a MAPK-related kinase. FASEB J. 2019:fj201802375RR. Epub 2019/02/23. https://doi.org/10.1096/fj.201802375RR PMID: 30794426.

41. Burghoorn J, Dekkers MP, Rademakers S, de Jong T, Willemsen R, Jansen G. Mutation of the MAP kinase DYF-5 affects docking and undocking of kinesin-2 motors and reduces their speed in the cilia of Caenorhabditis elegans. Proc Natl Acad Sci U S A. 2007; 104(17):7157–62. Epub 2007/04/11. https://doi.org/10.1073/pnas.0606974104 PMID: 17420466; PubMed Central PMCID: PMC1855366.

42. Chaya T, Omori Y, Kuwahara R, Furukawa T. ICK is essential for cell type-specific ciliogenesis and the regulation of ciliary transport. EMBO J. 2014; 33(11):1227–42. https://doi.org/10.1002/embj.201488175 PMID: 24797473; PubMed Central PMCID: PMC4198026.

43. Yang Y, Roine N, Makela TP. CCRK depletion inhibits glioblastoma cell proliferation in a cilium-dependent manner. EMBO reports. 2013; 14(8):741–7. https://doi.org/10.1038/embor.2013.80 PMID: 23743448; PubMed Central PMCID: PMC3736126.

44. Bengs F, Scholz A, Kuhn D, Wiese M. LmxMPK9, a mitogen-activated protein kinase homologue affects flagellar length in Leishmania mexicana. Mol Microbiol. 2005; 55(5):1606–15. Epub 2005/02/22. https://doi.org/10.1111/j.1365-2958.2005.04498.x PMID: 15720564.

45. Chen N, Mah A, Blacque OE, Chu J, Phgora K, Bakhoum MW, et al. Identification of ciliary and ciliopathy genes in Caenorhabditis elegans through comparative genomics. Genome biology. 2006; 7(12): R126. Epub 2006/12/26. https://doi.org/10.1186/gb-2006-7-12-r126 PMID: 17187676; PubMed Central PMCID: PMC1794439.

46. Yi P, Xie C, Ou G. The kinases male germ cell-associated kinase and cell cycle-related kinase regulate kinesin-2 motility in Caenorhabditis elegans neuronal cilia. Traffic. 2018; 19(7):522–35. Epub 2018/04/15. https://doi.org/10.1111/tra.12572 PMID: 29655266.

47. Tam LW, Wilson NF, Lefebvre PA. A CDK-related kinase regulates the length and assembly of flagella in Chlamydomonas. J Cell Biol. 2007; 176(6):819–29. Epub 2007/03/14. https://doi.org/10.1083/jcb.200610022 PMID: 17353359; PubMed Central PMCID: PMC2064056.

48. Phirke P, Efimenko E, Mohan S, Burghoorn J, Crona F, Bakhoum MW, et al. Transcriptional profiling of C. elegans DAF-19 uncovers a ciliary base-associated protein and a CDK/CCRK/LF2p-related kinase required for intraflagellar transport. Dev Biol. 2011; 357(1):235–47. https://doi.org/10.1016/j.ydbio.2011.06.028 PMID: 21740898; PubMed Central PMCID: PMC3888451.

49. Bradley BA, Quarmby LM. A NIMA-related kinase, Cnk2p, regulates both flagellar length and cell size in Chlamydomonas. J Cell Sci. 2005; 118(Pt 15):3317–26. https://doi.org/10.1242/jcs.02455 PMID: 16030138.

50. Wloga D, Camba A, Rogowski K, Manning G, Jerka-Dziadosz M, Gaertig J. Members of the NIMA-related kinase family promote disassembly of cilia by multiple mechanisms. Mol Biol Cell. 2006; 17(6):2799–810. Epub 2006/04/14. https://doi.org/10.1091/mbc.E05-05-0450 PMID: 16611747; PubMed Central PMCID: PMC1474788.

51. Meng D, Pan J. A NIMA-related kinase, CNK4, regulates ciliary stability and length. Mol Biol Cell. 2016; 27(5):838–47. https://doi.org/10.1091/mbc.E15-10-0707 PMID: 26764095; PubMed Central PMCID: PMC4803309.

52. Lin H, Zhang Z, Guo S, Chen F, Kessler JM, Wang YM, et al. A NIMA-Related Kinase Suppresses the Flagellar Instability Associated with the Loss of Multiple Axonemal Structures. PLoS Genet. 2015; 11(9):e1005508. Epub 2015/09/09. https://doi.org/10.1371/journal.pgen.1005508 PMID: 26348919; PubMed Central PMCID: PMC4562644.

53. Tam LW, Ranum PT, Lefebvre PA. CDKL5 regulates flagellar length and localizes to the base of the flagella in Chlamydomonas. Mol Biol Cell. 2013; 24(5):588–600. Epub 2013/01/04. https://doi.org/10.1091/mbc.E12-10-0718 PMID: 23283985; PubMed Central PMCID: PMC3583663.

54. Lefebvre PA, Nordstrom SA, Moulder JE, Rosenbaum JL. Flagellar elongation and shortening in Chlamydomonas. IV. Effects of flagellar detachment, regeneration, and resorption on the induction of flagellar protein synthesis. J Cell Biol. 1978; 78(1):8–27. Epub 1978/07/01. https://doi.org/10.1083/jcb.78.1.8 PMID: 149796; PubMed Central PMCID: PMC2110168.

55. Pan J, Wang Q, Snell WJ. An aurora kinase is essential for flagellar disassembly in Chlamydomonas. Dev Cell. 2004; 6(3):445–51. PMID: 15030766

56. Abdul-Majeed S, Moloney BC, Nauli SM. Mechanisms regulating cilia growth and cilia function in endothelial cells. Cellular and molecular life sciences: CMLS. 2012; 69(1):165–73. Epub 2011/06/15. https://doi.org/10.1007/s00018-011-0744-0 PMID: 21671118.

57. Liang YW, Zhu X, Wu Q, Pan JM. Ciliary Length Sensing Regulates IFT Entry via Changes in FLA8/KIF3B Phosphorylation to Control Ciliary Assembly. Current Biology. 2018; 28(15):2429–+. PubMed PMID: WOS:000440787800022. https://doi.org/10.1016/j.cub.2018.05.069 PMID: 30057303

58. Maskey D, Marlin MC, Kim S, Kim S, Ong EC, Li G, et al. Cell cycle-dependent ubiquitylation and destruction of NDE1 by CDK5-FBW7 regulates ciliary length. EMBO J. 2015; 34(19):2424–40. Epub 2015/07/25. https://doi.org/10.15252/embj.201490831 PMID: 26206584; PubMed Central PMCID: PMC4601663.

59. Husson H, Moreno S, Smith LA, Smith MM, Russo RJ, Pitstick R, et al. Reduction of ciliary length through pharmacologic or genetic inhibition of CDK5 attenuates polycystic kidney disease in a model of nephronophthisis. Hum Mol Genet. 2016; 25(11):2245–55. Epub 2016/10/30. https://doi.org/10.1093/hmg/ddw093 PMID: 27053712; PubMed Central PMCID: PMC5081056.

60. Liang Y, Pang Y, Wu Q, Hu Z, Han X, Xu Y, et al. FLA8/KIF3B phosphorylation regulates kinesin-II interaction with IFT-B to control IFT entry and turnaround. Dev Cell. 2014; 30(5):585–97. Epub 2014/09/02. https://doi.org/10.1016/j.devcel.2014.07.019 PMID: 25175706.

61. Keeling J, Tsiokas L, Maskey D. Cellular Mechanisms of Ciliary Length Control. Cells. 2016; 5(1). Epub 2016/02/04. https://doi.org/10.3390/cells5010006 PMID: 26840332; PubMed Central PMCID: PMC4810091.

62. Avasthi P, Marshall WF. Stages of ciliogenesis and regulation of ciliary length. Differentiation. 2012; 83 (2):S30–42. Epub 2011/12/20. https://doi.org/10.1016/j.diff.2011.11.015 PMID: 22178116; PubMed Central PMCID: PMC3269565.

63. Ludington WB, Ishikawa H, Serebrenik YV, Ritter A, Hernandez-Lopez RA, Gunzenhauser J, et al. A systematic comparison of mathematical models for inherent measurement of ciliary length: how a cell can measure length and volume. Biophys J. 2015; 108(6):1361–79. https://doi.org/10.1016/j.bpj.2014.12.051 PMID: 25809250; PubMed Central PMCID: PMC4375445.

64. Asleson CM, Lefebvre PA. Genetic analysis of flagellar length control in Chlamydomonas reinhardtii: a new long-flagella locus and extragenic suppressor mutations. Genetics. 1998; 148(2):693–702. Epub 1998/03/20. PMID: 9504917; PubMed Central PMCID: PMC1459834.

65. Wloga D, Frankel J. From molecules to morphology: cellular organization of Tetrahymena thermophila. Methods Cell Biol. 2012; 109:83–140. Epub 2012/03/27. https://doi.org/10.1016/B978-0-12-385967-9.00005-0 PMID: 22444144.

66. Bakowska J, Nelsen EM, Frankel J. Development of the Ciliary Pattern of the Oral Apparatus of Tetrahymena thermophila. J Protozool. 1982; 29:366–82.

67. Nelsen EM, Frankel J, Martel E. Development of the ciliature of Tetrahymena thermophila. I. Temporal coordination with oral development. Dev Biol. 1981; 88:27–38. https://doi.org/10.1016/0012-1606(81)90216-5 PMID: 7286446

68. Hanks SK, Hunter T. Protein kinases 6. The eukaryotic protein kinase superfamily: kinase (catalytic) domain structure and classification. FASEB J. 1995; 9(8):576–96. Epub 1995/05/01. PMID: 7768349.

69. Wolfe J, Grimes GW. Tip transformaton in Tetrahymena: morphogenetic response to interactions between mating types. J Protozool. 1979; 26:82–9.

70. Kiersnowska M, Kaczanowski A. Inhibition of oral morphogenesis during conjugation of Tetrahymena thermophila and its resumption after cell separation. Eur J Protistology. 1993; 29:359–69.

71. Pucciarelli S, Ballarini P, Sparvoli D, Barchetta S, Yu T, Detrich HW 3rd, et al. Distinct functional roles of beta-tubulin isotypes in microtubule arrays of Tetrahymena thermophila, a model single-celled organism. PLoS One. 2012; 7(6):e39694. https://doi.org/10.1371/journal.pone.0039694 PMID: 22745812; PubMed Central PMCID: PMC3382179.

72. Xiong J, Lu X, Zhou Z, Chang Y, Yuan D, Tian M, et al. Transcriptome analysis of the model protozoan, Tetrahymena thermophila, using Deep RNA sequencing. PLoS One. 2012; 7(2):e30630. Epub 2012/02/22. https://doi.org/10.1371/journal.pone.0030630 PMID: 22347391; PubMed Central PMCID: PMC3274533.

73. Shang Y, Song X, Bowen J, Corstanje R, Gao Y, Gaertig J, et al. A robust inducible-repressible promoter greatly facilitates gene knockouts, conditional expression, and overexpression of homologous and heterologous genes in Tetrahymena thermophila. Proc Natl Acad Sci U S A. 2002; 99(6):3734–9. Epub 2002/03/14. https://doi.org/10.1073/pnas.052016199 PMID: 11891286; PubMed Central PMCID: PMC122593.

74. Brown JM, Hardin C, Gaertig J. Rotokinesis, a novel phenomenon of cell locomotion-assisted cytokinesis in the ciliate Tetrahymena thermophila. Cell Biol Int. 1999; 23(12):841–8. Epub 2000/04/25. https://doi.org/10.1006/cbir.1999.0480 PMID: 10772758.

75. Jain RK, Joyce PB, Molinete M, Halban PA, Gorr SU. Oligomerization of green fluorescent protein in the secretory pathway of endocrine cells. Biochem J. 2001; 360(Pt 3):645–9. Epub 2001/12/12. https://doi.org/10.1042/0264-6021:3600645 PMID: 11736655; PubMed Central PMCID: PMC1222268.

76. Jiang YY, Lechtreck K, Gaertig J. Total internal reflection fluorescence microscopy of intraflagellar transport in Tetrahymena thermophila. Methods Cell Biol. 2015; 127:445–56. Epub 2015/04/04.

https://doi.org/10.1016/bs.mcb.2015.01.001 PMID: 25837403; PubMed Central PMCID: PMC5301313.

77. Fan ZC, Behal RH, Geimer S, Wang Z, Williamson SM, Zhang H, et al. Chlamydomonas IFT70/CrDYF-1 is a core component of IFT particle complex B and is required for flagellar assembly. Mol Biol Cell. 2010; 21(15):2696–706. Epub 2010/06/11. https://doi.org/10.1091/mbc.E10-03-0191 PMID: 20534810; PubMed Central PMCID: PMC2912355.

78. Piperno G, Mead K. Transport of a novel complex in the cytoplasmic matrix of *Chlamydomonas* flagella. Proc Natl Acad Sci USA. 1997; 94:4457–62. https://doi.org/10.1073/pnas.94.9.4457 PMID: 9114011

79. Cole ES, Bruns PJ. Uniparental cytogamy: A novel method for bringing micronuclear mutations of tetrahymena into homozygous macronuclear expression with precocious sexual maturity. Genetics. 1992; 132:1017–31. PMID: 1459424

80. Artz JD, Wernimont AK, Allali-Hassani A, Zhao Y, Amani M, Lin YH, et al. The Cryptosporidium parvum kinome. BMC genomics. 2011; 12:478. Epub 2011/10/04. https://doi.org/10.1186/1471-2164-12-478 PMID: 21962082; PubMed Central PMCID: PMC3227725.

81. Fiser A, Do RK, Sali A. Modeling of loops in protein structures. Protein Sci. 2000; 9(9):1753–73. Epub 2000/10/25. https://doi.org/10.1110/ps.9.9.1753 PMID: 11045621; PubMed Central PMCID: PMC2144714.

82. Torkamani A, Kannan N, Taylor SS, Schork NJ. Congenital disease SNPs target lineage specific structural elements in protein kinases. Proc Natl Acad Sci U S A. 2008; 105(26):9011–6. Epub 2008/06/27. https://doi.org/10.1073/pnas.0802403105 PMID: 18579784; PubMed Central PMCID: PMC2449356.

83. Jiang YY, Maier W, Baumeister R, Minevich G, Joachimiak E, Ruan Z, et al. The Hippo Pathway Maintains the Equatorial Division Plane in the Ciliate Tetrahymena. Genetics. 2017; 206(2):873–88. Epub 2017/04/18. https://doi.org/10.1534/genetics.117.200766 PMID: 28413159; PubMed Central PMCID: PMC5499192.

84. Ohnishi J, Mizoguchi H, Takeno S, Ikeda M. Characterization of mutations induced by N-methyl-N'-nitro-N-nitrosoguanidine in an industrial Corynebacterium glutamicum strain. Mutat Res. 2008; 649(1–2):239–44. https://doi.org/10.1016/j.mrgentox.2007.10.003 PMID: 18037338.

85. McSkimming DI, Rasheed K, Kannan N. Classifying kinase conformations using a machine learning approach. BMC bioinformatics. 2017; 18(1):86. Epub 2017/02/06. https://doi.org/10.1186/s12859-017-1506-2 PMID: 28152981; PubMed Central PMCID: PMC5290640.

86. Talevich E, Kannan N. Structural and evolutionary adaptation of rhoptry kinases and pseudokinases, a family of coccidian virulence factors. BMC Evol Biol. 2013; 13:117. Epub 2013/06/08. https://doi.org/10.1186/1471-2148-13-117 PMID: 23742205; PubMed Central PMCID: PMC3682881.

87. Pratt DJ, Bentley J, Jewsbury P, Boyle FT, Endicott JA, Noble ME. Dissecting the determinants of cyclin-dependent kinase 2 and cyclin-dependent kinase 4 inhibitor selectivity. Journal of medicinal chemistry. 2006; 49(18):5470–7. Epub 2006/09/01. https://doi.org/10.1021/jm060216x PMID: 16942020.

88. Drozdetskiy A, Cole C, Procter J, Barton GJ. JPred4: a protein secondary structure prediction server. Nucleic Acids Res. 2015; 43(W1):W389–94. Epub 2015/04/18. https://doi.org/10.1093/nar/gkv332 PMID: 25883141; PubMed Central PMCID: PMC4489285.

89. Orias E, Rasmussen L. Dual capacity for nutrient uptake in tetrahymena. IV. growth without food vacuoles. Exp Cell Res. 1976; 102:127–37. https://doi.org/10.1016/0014-4827(76)90307-4 PMID: 824146

90. Irniger S. The Ime2 protein kinase family in fungi: more duties than just meiosis. Mol Microbiol. 2011; 80(1):1–13. Epub 2011/02/11. https://doi.org/10.1111/j.1365-2958.2011.07575.x PMID: 21306447.

91. Aury JM, Jaillon O, Duret L, Noel B, Jubin C, Porcel BM, et al. Global trends of whole-genome duplications revealed by the ciliate Paramecium tetraurelia. Nature. 2006; 444(7116):171–8. https://doi.org/10.1038/nature05230 PMID: 17086204.

92. Mitchell DR. The evolution of eukaryotic cilia and flagella as motile and sensory organelles. Advances in experimental medicine and biology. 2007; 607:130–40. Epub 2007/11/06. https://doi.org/10.1007/978-0-387-74021-8_11 PMID: 17977465; PubMed Central PMCID: PMC3322410.

93. Snouffer A, Brown D, Lee H, Walsh J, Lupu F, Norman R, et al. Cell Cycle-Related Kinase (CCRK) regulates ciliogenesis and Hedgehog signaling in mice. PLoS Genet. 2017; 13(8):e1006912. Epub 2017/08/18. https://doi.org/10.1371/journal.pgen.1006912 PMID: 28817564; PubMed Central PMCID: PMC5574612.

94. Barsel SE, Wexler DE, Lefebvre PA. Genetic analysis of long-flagella mutants of Chlamydomonas reinhardtii. Genetics. 1988; 118:637–48. PMID: 3366366

95. Omori Y, Chaya T, Katoh K, Kajimura N, Sato S, Muraoka K, et al. Negative regulation of ciliary length by ciliary male germ cell-associated kinase (Mak) is required for retinal photoreceptor survival. Proc Natl Acad Sci U S A. 2010; 107(52):22671–6. Epub 2010/12/15. https://doi.org/10.1073/pnas.1009437108 PMID: 21148103; PubMed Central PMCID: PMC3012466.

96. Dentler W. Intraflagellar transport (IFT) during assembly and disassembly of Chlamydomonas flagella. J Cell Biol. 2005; 170(4):649–59. Epub 2005/08/17. https://doi.org/10.1083/jcb.200412021 PMID: 16103230; PubMed Central PMCID: PMC2171492.

97. Wingfield JL, Mengoni I, Bomberger H, Jiang YY, Walsh JD, Brown JM, et al. IFT trains in different stages of assembly queue at the ciliary base for consecutive release into the cilium. Elife. 2017; 6. Epub 2017/06/01. https://doi.org/10.7554/eLife.26609 PMID: 28562242; PubMed Central PMCID: PMC5451262.

98. Fu Z, Larson KA, Chitta RK, Parker SA, Turk BE, Lawrence MW, et al. Identification of yin-yang regulators and a phosphorylation consensus for male germ cell-associated kinase (MAK)-related kinase. Molecular and cellular biology. 2006; 26(22):8639–54. Epub 2006/09/07. https://doi.org/10.1128/MCB.00816-06 PMID: 16954377; PubMed Central PMCID: PMC1636783.

99. Fu Z, Schroeder MJ, Shabanowitz J, Kaldis P, Togawa K, Rustgi AK, et al. Activation of a nuclear Cdc2-related kinase within a mitogen-activated protein kinase-like TDY motif by autophosphorylation and cyclin-dependent protein kinase-activating kinase. Molecular and cellular biology. 2005; 25 (14):6047–64. Epub 2005/07/01. https://doi.org/10.1128/MCB.25.14.6047-6064.2005 PMID: 15988018; PubMed Central PMCID: PMC1168834.

100. Wu D, Chapman JR, Wang L, Harris TE, Shabanowitz J, Hunt DF, et al. Intestinal cell kinase (ICK) promotes activation of mTOR complex 1 (mTORC1) through phosphorylation of Raptor Thr-908. J Biol Chem. 2012; 287(15):12510–9. Epub 2012/02/24. https://doi.org/10.1074/jbc.M111.302117 PMID: 22356909; PubMed Central PMCID: PMC3321000.

101. Wang LY, Kung HJ. Male germ cell-associated kinase is overexpressed in prostate cancer cells and causes mitotic defects via deregulation of APC/CCDH1. Oncogene. 2012; 31(24):2907–18. Epub 2011/10/12. https://doi.org/10.1038/onc.2011.464 PMID: 21986944; PubMed Central PMCID: PMC3566783.

102. Jeanmougin F, Thompson JD, Gouy M, Higgins DG, Gibson TJ. Multiple sequence alignment with Clustal X. Trends Biochem Sci. 1998; 23(10):403–5. PMID: 9810230.

103. Galtier N, Gouy M, Gautier C. SEAVIEW and PHYLO_WIN: two graphic tools for sequence alignment and molecular phylogeny. Comput Appl Biosci. 1996; 12(6):543–8. PMID: 9021275.

104. Felsenstein J. PHYLIP (Phylogeny Inference Package) version 3.6. Distributed by the author. Department of Genome Sciences, University of Washington, Seattle. 2005.

105. Gorovsky MA. Studies on nuclear structure and function in Tetrahymena pyriformis II Isolation of macro- and micronuclei. JCell Biol. 1970; 47:619–30. https://www.ncbi.nlm.nih.gov/pmc/articles/PMC2108162/

106. Dave D, Wloga D, Gaertig J. Manipulating ciliary protein-encoding genes in Tetrahymena thermophila. Methods Cell Biol. 2009; 93:1–20. Epub 2009/01/01. https://doi.org/10.1016/S0091-679X(08)93001-6 PMID: 20409809.

107. Gaertig J, Wloga D, Vasudevan KK, Guha M, Dentler WL. Discovery and functional evaluation of ciliary proteins in Tetrahymena thermophila. In: Marshall WF, editor. Cilia, part B. Methods in Enzymology. 2552013. https://doi.org/10.1016/B978-0-12-397944-5.10000-8

108. Busch CJ, Vogt A, Mochizuki K. Establishment of a Cre/loxP recombination system for N-terminal epitope tagging of genes in Tetrahymena. BMC microbiology. 2010; 10:191. Epub 2010/07/16. https://doi.org/10.1186/1471-2180-10-191 PMID: 20626890; PubMed Central PMCID: PMC2912859.

109. Urbanska P, Song K, Joachimiak E, Krzemien-Ojak L, Koprowski P, Hennessey T, et al. The CSC proteins FAP61 and FAP251 build the basal substructures of radial spoke 3 in cilia. Mol Biol Cell. 2015; 26 (8):1463–75. https://doi.org/10.1091/mbc.E14-11-1545 PMID: 25694453.

110. Iwamoto M, Mori C, Hiraoka Y, Haraguchi T. Puromycin resistance gene as an effective selection marker for ciliate Tetrahymena. Gene. 2014; 534(2):249–55. Epub 2013/11/05. https://doi.org/10.1016/j.gene.2013.10.049 PMID: 24185080

111. Mochizuki K. High efficiency transformation of Tetrahymena using a codon-optimized neomycin resistance gene. Gene. 2008; 425(1–2):79–83. Epub 2008/09/09. doi: S0378-1119(08)00394-6 [pii] https://doi.org/10.1016/j.gene.2008.08.007 PMID: 18775482.

112. Gaertig J, Gao Y, Tishgarten T, Clark TG, Dickerson HW. Surface display of a parasite antigen in the ciliate Tetrahymena thermophila. Nat Biotechnol. 1999; 17(5):462–5. Epub 1999/05/20. https://doi.org/10.1038/8638 PMID: 10331805.

113. Dave D, Wloga D, Sharma N, Gaertig J. DYF-1 Is required for assembly of the axoneme in Tetrahymena thermophila. Eukaryot Cell. 2009; 8(9):1397–406. Epub 2009/07/08. https://doi.org/10.1128/EC.00378-08 PMID: 19581442; PubMed Central PMCID: PMC2747827.

114. Kataoka K, Schoeberl UE, Mochizuki K. Modules for C-terminal epitope tagging of Tetrahymena genes. Journal of microbiological methods. 2010; 82(3):342–6. Epub 2010/07/14. https://doi.org/10.1016/j.mimet.2010.07.009 PMID: 20624430; PubMed Central PMCID: PMC2935961.

115. Bruns PJ, Brussard TB, Kavka AB. Isolation of homozygous mutants after induced self-fertilization in Tetrahymena. Proc Natl Acad Sci U S A. 1976; 73(9):3243–7. https://doi.org/10.1073/pnas.73.9.3243 PMID: 823548; PubMed Central PMCID: PMC430993.

116. Schindelin J, Arganda-Carreras I, Frise E, Kaynig V, Longair M, Pietzsch T, et al. Fiji: an open-source platform for biological-image analysis. Nature methods. 2012; 9(7):676–82. Epub 2012/06/30. https://doi.org/10.1038/nmeth.2019 PMID: 22743772; PubMed Central PMCID: PMC3855844.

117. Candiano G, Bruschi M, Musante L, Santucci L, Ghiggeri GM, Carnemolla B, et al. Blue silver: a very sensitive colloidal Coomassie G-250 staining for proteome analysis. Electrophoresis. 2004; 25 (9):1327–33. Epub 2004/06/03. https://doi.org/10.1002/elps.200305844 PMID: 15174055.

118. Dryl S. Antigenic transformation in Paramecium aurelia after homologous antiserum treatment during autogamy and conjugation. J Protozool. 1959; 6:25.

119. Gaertig J, Thatcher TH, Gu L, Gorovsky MA. Electroporation-mediated replacement of a positively and negatively selectable b-tubulin gene in *Tetrahymena thermophila*. Proc Natl Acad Sci USA. 1994; 91:4549–53. https://doi.org/10.1073/pnas.91.10.4549 PMID: 7910408

120. Eisen JA, Coyne RS, Wu M, Wu D, Thiagarajan M, Wortman JR, et al. Macronuclear genome sequence of the ciliate Tetrahymena thermophila, a model eukaryote. PLOS Biol. 2006; 4(9):e286. Epub 2006/08/29. https://doi.org/10.1371/journal.pbio.0040286 PMID: 16933976; PubMed Central PMCID: PMC1557398.

121. Hamilton EP, Kapusta A, Huvos PE, Bidwell SL, Zafar N, Tang H, et al. Structure of the germline genome of Tetrahymenathermophila and relationship to the massively rearranged somatic genome. Elife. 2016;5. https://doi.org/10.7554/eLife.19090 PMID: 27892853.

122. Maier W, Moos K, Seifert M, Baumeister R. Mutation Identification in Model Organism Genomes [Computer Software]: SourceForge.net; 2014. 0.1.8:[Available from: https://sourceforge.net/projects/mimodd/.]. 2014.

123. Kannan N, Taylor SS, Zhai Y, Venter JC, Manning G. Structural and functional diversity of the microbial kinome. PLoS Biol. 2007; 5(3):e17. Epub 2007/03/16. https://doi.org/10.1371/journal.pbio.0050017 PMID: 17355172; PubMed Central PMCID: PMC1821047.

124. Talevich E, Mirza A, Kannan N. Structural and evolutionary divergence of eukaryotic protein kinases in Apicomplexa. BMC Evol Biol. 2011; 11:321. Epub 2011/11/04. https://doi.org/10.1186/1471-2148-11-321 PMID: 22047078; PubMed Central PMCID: PMC3239843.

125. Neuwald AF. Rapid detection, classification and accurate alignment of up to a million or more related protein sequences. Bioinformatics. 2009; 25(15):1869–75. Epub 2009/06/10. https://doi.org/10.1093/bioinformatics/btp342 PMID: 19505947; PubMed Central PMCID: PMC2732367.

126. Eddy SR. Accelerated Profile HMM Searches. PLoS Comput Biol. 2011; 7(10):e1002195. Epub 2011/11/01. https://doi.org/10.1371/journal.pcbi.1002195 PMID: 22039361; PubMed Central PMCID: PMC3197634.

127. Manning G, Whyte DB, Martinez R, Hunter T, Sudarsanam S. The protein kinase complement of the human genome. Science. 2002; 298(5600):1912–34. Epub 2002/12/10. https://doi.org/10.1126/science.1075762 PMID: 12471243.

128. Madden T. The BLAST Sequence Analysis Tool. In: McEntyre J, Ostell J, editors. The NCBI Handbook [Internet]. Bethesda (MD): National Center for Biotechnology Information (US); 2002.

129. Schrodinger LLC. The PyMOL Molecular Graphics System, Version 1.8. 2015.

130. Zhang Y. I-TASSER: fully automated protein structure prediction in CASP8. Proteins. 2009; 77 Suppl 9:100–13. Epub 2009/09/22. https://doi.org/10.1002/prot.22588 PMID: 19768687; PubMed Central PMCID: PMC2782770.

131. Roy A, Yang J, Zhang Y. COFACTOR: an accurate comparative algorithm for structure-based protein function annotation. Nucleic Acids Res. 2012; 40(Web Server issue):W471–7. Epub 2012/05/10. https://doi.org/10.1093/nar/gks372 PMID: 22570420; PubMed Central PMCID: PMC3394312.

132. Yang J, Zhang Y. I-TASSER server: new development for protein structure and function predictions. Nucleic Acids Res. 2015; 43(W1):W174–81. Epub 2015/04/18. https://doi.org/10.1093/nar/gkv342 PMID: 25883148; PubMed Central PMCID: PMC4489253.